

PROPERTIES OF THE TRANS-NEPTUNIAN BELT: STATISTICS FROM THE CFHT SURVEY¹

Chadwick A. Trujillo²

Institute for Astronomy, 2680 Woodlawn Drive, Honolulu, HI 96822
chad@ifa.hawaii.edu

David C. Jewitt

Institute for Astronomy, 2680 Woodlawn Drive, Honolulu, HI 96822
jewitt@ifa.hawaii.edu

and

Jane X. Luu

Leiden Observatory, PO Box 9513, 2300 RA Leiden, The Netherlands
luu@strw.leidenuniv.nl

ABSTRACT

We present the results of a wide-field survey designed to measure the size, inclination, and radial distributions of Kuiper Belt Objects (KBOs). The survey found 86 KBOs in 73 square degrees observed to limiting red magnitude 23.7 using the Canada-France-Hawaii Telescope and the 12k x 8k CCD Mosaic camera. For the first time, both ecliptic and off-ecliptic fields were examined to more accurately constrain the inclination distribution of the KBOs. The survey data were processed using an automatic moving object detection algorithm, allowing a careful characterization of the biases involved. In this work, we quantify fundamental parameters of the Classical KBOs (CKBOs), the most numerous objects found in our sample, using the new data and a maximum likelihood simulation. Deriving results from our best-fit model, we find that the size distribution follows a differential power law with exponent $q = 4.0^{+0.6}_{-0.5}$ (1σ , or 68.27% confidence). In addition, the CKBOs inhabit a very thick disk consistent with a Gaussian distribution of inclinations with a Half-Width of $i_{1/2} = 20^{+6}_{-4}^\circ$.

¹Based on observations collected at Canada-France-Hawaii Telescope, which is operated by the National Research Council of Canada, the Centre National de la Recherche Scientifique de France, and the University of Hawaii.

²Now at California Institute of Technology, MS 150-21, Pasadena, CA 91125. chad@gps.caltech.edu

(1 σ). We estimate that there are $N_{\text{CKBOs}}(D > 100 \text{ km}) = 3.8^{+2.0}_{-1.5} \times 10^4$ (1 σ) CKBOs larger than 100 km in diameter. We also find compelling evidence for an outer edge to the CKBOs at heliocentric distance $R = 50 \text{ AU}$.

Subject headings: Kuiper Belt, Oort Cloud — minor planets, asteroids — solar system: formation

1. Introduction

The rate of discovery of Kuiper Belt Objects (KBOs) has increased dramatically since the first member (1992 QB₁) was found (Jewitt & Luu 1993). As of Dec 2000, ~ 400 KBOs are known. These bodies exist in three dynamical classes (Jewitt, Luu & Trujillo 1998): (1) the Classical KBOs (CKBOs) occupy nearly circular (eccentricities $e < 0.25$) orbits with semimajor axes $41 \text{ AU} \lesssim a \lesssim 46 \text{ AU}$, and they constitute $\sim 70 \%$ of the observed population; (2) the Resonant KBOs occupy mean-motion resonances with Neptune, such as the 3:2 (the Plutinos, $a \approx 39.4 \text{ AU}$) and 2:1 ($a \approx 47.8 \text{ AU}$), and comprise $\sim 20 \%$ of the known objects; (3) the Scattered KBOs represent only $\sim 10 \%$ of the known KBOs, but possess the most extreme orbits, with median semimajor axis $a \sim 90 \text{ AU}$ and eccentricity $e \sim 0.6$, presumably due to a weak interaction with Neptune (Duncan & Levison 1997, Luu et al. 1997, and Trujillo, Jewitt & Luu 2000). Although these classes are now well established, only rudimentary information has been collected about their populations. One reason is that only a fraction of the known KBOs were discovered in well-parametrized surveys that have been published in the open literature (principally Jewitt & Luu 1993 (1 KBO); Jewitt & Luu 1995 (17 KBOs); Irwin, Tremaine & Żytkow 1995 (2 KBOs); Jewitt, Luu & Chen 1996 (15 KBOs); Gladman et al. 1998 (5 KBOs); Jewitt, Luu & Trujillo 1998 (13 KBOs); and Chiang & Brown 1999 (2 KBOs)). In this work, we characterize the fundamental parameters of the CKBOs: the size distribution, inclination distribution and radial distribution using a large sample (86 KBOs) discovered in a well-characterized survey.

The quintessential measurement of the size distribution relies on the Cumulative Luminosity Function (CLF). The CLF describes the number of KBOs deg^{-2} (Σ) near the ecliptic as a function of apparent red magnitude (m_R). It is fitted with the relation $\log(\Sigma) = \alpha(m_R - m_0)$, where m_0 is the red magnitude at which $\Sigma = 1 \text{ KBO deg}^{-2}$. The slope (α) is related to the size distribution (described later). Although many different works have considered the CLF, two papers are responsible for discovering the majority of KBOs found in published surveys: Jewitt, Luu & Chen (1996) and Jewitt, Luu & Trujillo

(1998). The former constrained the CLF over a 1.6 magnitude range ($23.2 < m_R < 24.8$) with 15 discovered KBOs while the latter covered a complimentary 2.5 magnitude range ($20.5 < m_R < 23.0$), discovering 13 objects. Jewitt, Luu & Trujillo (1998) measured the CLF produced from these two data sets and found $\alpha = 0.58 \pm 0.05$ and $m_0 = 23.27 \pm 0.11$. Gladman et al. (1998) criticized this work on 2 main counts: (1) they believed that Jewitt, Luu & Chen (1996) underestimated the number of KBOs and (2) the fit in the Jewitt, Luu & Trujillo (1998) survey used a least-squares approach that assumed Gaussian errors rather than Poissonian errors. Gladman et al. (1998) found 5 additional KBOs and re-analysed the CLF using a Poissonian maximum likelihood method to refit the CLF to (1) the Jewitt, Luu & Trujillo (1998) data without the Jewitt, Luu & Chen (1996) data and (2) a fit to the 6 different surveys available at the time except for Tombaugh (1961), Kowal (1989) and Jewitt, Luu & Chen (1996). Both of these fits were steeper but formally consistent with the original Jewitt, Luu & Trujillo (1998) data at the $\sim 1.5\sigma$ level: (1) $\alpha = 0.72^{+0.30}_{-0.26}$ and $m_0 = 23.3^{+0.2}_{-0.4}$ and (2) $\alpha = 0.76^{+0.10}_{-0.11}$ and $m_0 = 23.40^{+0.20}_{-0.18}$. Chiang & Brown (1999) find a flatter size distribution of $\alpha = 0.52 \pm 0.05$ and $m_0 = 23.5 \pm 0.06$ much closer to the Jewitt, Luu & Trujillo (1998) result. They observed that the steep size distribution reported by Gladman et al. (1998) was an artifact of their selective exclusion of part of the available survey data, not of their use of a different fitting method. The first goal of this work is to measure the CLF and additionally constrain the power-law slope of the size distribution using a single well-characterized survey and a maximum likelihood simulation which allows for the correction of observational biases.

An accurate characterization of the inclination distribution of the KBOs is critical to understanding the dynamical history of the outer Solar System since the era of planetesimal formation. We expect that the KBOs formed by accretion in a very thin disk of particles with a small internal velocity dispersion (e.g. Kenyon & Luu 1998 and Hahn & Malhotra 1999) and a correspondingly small inclination distribution. However, the velocity dispersion indicated by the inclination distribution in the present-day Kuiper Belt is large. Jewitt, Luu & Chen (1996) measured the *apparent* Half-Width of the Kuiper Belt inclination distribution to be $\sim 5^\circ$. They noted a strong bias against observing high inclination objects in ecliptic surveys, and they estimated the true distribution to be much thicker, with an inclination distribution Half-Width of $\gtrsim 15^\circ$, corresponding to a vertical velocity dispersion of ~ 1 km/s. Several conjectures have been advanced to explain the thickness of the Kuiper Belt: Earth-mass planetesimals may have been scattered through the belt in the late stages of the planet-formation era, exciting the Kuiper Belt (Morbidelli & Valsecchi 1997 and Petit et al. 1999); stellar encounters may have enhanced the velocity dispersion of the distant KBOs (Ida, Larwood & Burkert, 2000); and the dispersion velocity of small bodies tends to grow to roughly equal the escape speed of the bodies contributing the most mass (the large

bodies for size distributions with $q < 4$) in the belt (Aarseth, Lin & Palmer 1993). As there is much speculation about the origin of the large velocity dispersion of the Kuiper Belt, but only one published measurement (Jewitt, Luu & Chen 1996), the second goal of this work is to accurately quantify the inclination distribution from our large sample of objects.

The radial extent of the Classical Kuiper Belt has not been well constrained. None of the CKBOs have been discovered beyond $R \approx 50$ AU. This trend was first noted by Dones (1997) who suggested that the 50–75 AU region may be depleted; he found the results of a Monte-Carlo simulation of CKBOs drawn from a rather flat differential size distribution (power-law index $q = 3$) to be inconsistent with the observations of the 6 CKBOs discovered by Jewitt, Luu & Chen (1996). Jewitt, Luu & Trujillo (1998) discovered all of their KBOs at heliocentric distances $R < 46$ AU. In the absence of other effects, one should expect to find fewer bodies with $R > 50$ AU than with $R \sim 40$ AU, as the former are about a magnitude fainter than the latter. However, through the use of a Monte-Carlo model they demonstrated that the bias against objects beyond 50 AU is not strong enough to explain the distribution of discovery distances. They speculated that the lack of bodies discovered beyond 50 AU could be caused by a combination of (1) a decrease in the maximum KBO size (and reduction in the brightest and most detectable objects) beyond 50 AU or (2) the size distribution might steepen beyond 50 AU, putting more of the mass in the smaller, less-detectable bodies. They also suggested that the lack of $R > 50$ AU objects could be explained by an outer edge to the Classical Kuiper Belt at 50 AU.

Two later papers questioned the existence of an edge to the Kuiper Belt near 50 AU. Gladman et al. (1998) suggested that the number of objects expected to be discovered beyond 50 AU is highly dependent on the size distribution because steep size distributions reduce the number of large (bright) bodies relative to small (faint) bodies. Gladman et al. (1998) adopted a relatively steep distribution ($q = 4.65$), and found no significant evidence of a truncated belt. Chiang & Brown (1999) found that 8%–13% of the ~ 100 objects known at the time should have been found beyond 50 AU, and suggested that this precludes the presence of a density enhancement beyond 50 AU, but could not definitively rule out a density deficit. Allen, Bernstein & Malhotra (2001) have also recently reported the detection of an outer edge to the Kuiper Belt. The third goal of the present work is to test the distribution of the discovery distances for the presence of an outer edge to the Kuiper Belt.

2. Survey Data

Observations were made at the 3.6 m diameter Canada-France-Hawaii Telescope using the 12288 x 8192, 15 μm pixel mosaic CCD (CFHT 12k; Cuillandre et al. 2000). Built at the University of Hawaii (UH) the CFHT 12k comprises 12 edge-abutted, thinned, high quantum efficiency ($\text{QE} \sim 0.75$), 4096 x 2048 pixel Lincoln Laboratory CCDs. It is currently the largest close-packed CCD camera in the world. When mounted at the CFHT f/4 prime focus the camera yields a plate scale of 0.206 arc sec/pixel, corresponding to a 0.330 sq deg field of view in each 200 Mbyte image. Images were taken through a Mould R filter, with a central wavelength of 6581 Å and a bandwidth of 1251 Å. Instrumental parameters of the survey are summarized in Table 1.

Observations were taken within a few days of new moon under photometric conditions during three periods: Feb 10 – 15 1999, Sep 5–8 1999, and Mar 31 – Apr 3 2000. Fields were imaged at airmasses < 1.7 and were within 1.5 hours of opposition. We chose to use short 180 s exposures at the CFHT to maximize area coverage and detection statistics. All discovered objects were accessible for recovery at the UH 2.2 m telescope during comparable seeing conditions with exposure times of < 600 seconds. Each field was imaged three times (a “field triplet”), with about 1 hour timebase between exposures. Fields imaged appear in Figures 1, 2 and 3, and in Table 3. The CFHT observations were taken at three ecliptic latitudes $\beta = 0^\circ, 10^\circ$, and 20° to probe the inclination distribution of the KBOs (see §4).

Photometric calibrations were obtained from Landolt (1992) standard stars imaged several times on each chip. Three CFHT 12k chips of poor quality were replaced between the Feb 1999 and Sep 1999 runs. The positions of four other CFHT 12k chips within the focal plane array were changed to move the cosmetically superior chips towards the center of the camera. The photometric calibration accounts for these changes, as shown in Table 2, containing the measured photometric zero points of the chips. In addition, chip 6 was not used in Feb 1999 because of its extremely poor cosmetic quality. The area covered in the fields from Feb 1999 was corrected for this 8% reduction in field-of-view. The area imaged in Mar 2000 included some small field overlap (6%), resulting in a minor correction applied to the reported total area surveyed.

Each of the 12 CCDs in the CFHT 12k functions as an individual detector, with its own characteristic bias level, flat field, gain level, and orientation (at the $\sim 1^\circ$ level). The bias level for each chip was estimated using the row-by-row median of the overscan region. Flat fields were constructed from a combination of (1) the median of normalized bias-subtracted twilight flat fields and (2) a median of bias-subtracted data frames, with a clipping algorithm used to remove excess counts due to bright stars. Fields were analysed by subtracting the overscan region, dividing by the composite flats and searching for moving

objects using our Moving Object Detection Software (MODS, Trujillo & Jewitt 1998). We rejected bad pixels through the use of a bad pixel mask.

Artificial moving objects were added to the data to quantify the sensitivity of the moving object detection procedure (Trujillo & Jewitt 1998). The seeing during the survey typically varied from 0.7 arc sec to 1.1 arc sec (FWHM). Accordingly, we subdivided and analysed the data in 3 groups based on the seeing. Artificial moving objects were added to bias-subtracted twilight sky-flattened images, with profiles matched to the characteristic point-spread function for each image group. These images were then passed through the data analysis pipeline. The detection efficiency was found to be uniform with respect to sky-plane speed in the 1 – 10 arc sec/hr range. At opposition, the apparent speed in arc sec/hr, $\dot{\theta}$, of an object is dominated by the parallactic motion of the Earth, and follows

$$\dot{\theta} \approx 148 \left(\frac{1 - R^{-0.5}}{R - 1} \right), \quad (1)$$

where R is heliocentric distance in AU (Luu & Jewitt 1988). From Equation 1, our speed limit criterion for the survey, $1'' \text{ hr}^{-1} < \dot{\theta} < 10'' \text{ hr}^{-1}$, corresponds to opposition heliocentric distances $10 \text{ AU} \lesssim R \lesssim 140 \text{ AU}$, with efficiency variations within this range due only to object brightness and seeing.

The magnitude-dependent efficiency function was fitted by

$$\varepsilon = \frac{\varepsilon_{\max}}{2} \left(\tanh \left(\frac{m_{R50} - m_R}{\sigma} \right) + 1 \right), \quad (2)$$

where $0 < \varepsilon < 1$ is the efficiency with which objects of red magnitude m_R are detected, ε_{\max} is the maximum efficiency, m_{R50} is the magnitude at which $\varepsilon = \varepsilon_{\max}/2$, and σ magnitudes is the characteristic range over which the efficiency drops from ε_{\max} to zero. Table 4 shows the efficiency function derived for each seeing category, along with an average of the seeing cases, weighted by sky area imaged, applicable to the entire data set. The efficiency function is known to greater precision than the ~ 0.1 magnitude uncertainty on our discovery photometry. Changes to the efficiency function of < 0.1 magnitudes produce no significant variation in our results for the size or inclination distributions.

The MODS software, running on two Ultra 10 computers, was fast enough to efficiently search for the KBOs in near real-time, so that newly detected objects could be quickly discovered and re-imaged. We imaged ~ 35 field triplets each night at the CFHT, corresponding to ~ 20 Gbytes of raw data collected per night, plus several more Gbytes for flat fields and standard stars. Eighty-six KBOs were found in the CFHT survey, 2 of which were serendipitous re-detections of known objects. The discovery conditions of the detected objects appear in Table 5. Photometry was performed using a 2.5 arc second

diameter synthetic aperture for discovery data, resulting in median photometric error of 0.15 magnitudes and a maximum photometric error of 0.3 for the faintest objects. Our results are unaffected by this error; randomly introducing ± 0.15 magnitude errors in our simulations (described later), and ± 0.3 magnitude errors in the faintest objects produced no statistically significant change. Trailing loss was insignificant as the KBOs moved only 0.15 arc sec during our integration.

2.1. Recovery Observations and Orbits

Extensive efforts were made to recover all objects using the UH 2.2 m telescope. Attempts were made to recover the objects one week after discovery, then one, two and three months after discovery. Most of these attempts were successful, as demonstrated by the fact that 79 of the 86 CFHT objects were recovered. The loss of 7 objects is the result of unusually poor weather during the Mar–May 1999 recovery period. Only 6 of the 79 recovered objects have arc-lengths shorter than 30 days as of Dec 1, 2000. Second opposition observations have been acquired for 36 of the 78 KBOs found in Feb 1999 and Sep 1999.

Orbits derived from the discovery and recovery data appear in Table 6. The listed elements are those computed by Brian Marsden of the Minor Planet Center. We also benefited from orbital element calculations by David Tholen (Univ. of Hawaii). Both sources produced comparable orbital solutions to the astrometric data.

With only first opposition observations, the inclination and heliocentric distance at discovery can be well determined for nearly all KBOs, as depicted in Figure 4. We find that the semimajor axis and eccentricity determinations are less reliable but are usually good enough to classify the objects as either Classical, Resonance or Scattered KBOs, as depicted in Figure 5. We find that 6 out of 36 (17%) of the objects exhibit orbital changes large enough for their dynamical classification to change from the first opposition to the second opposition. Randomly rejecting 17% of our sample (to simulate misclassification) does not significantly change the results. In addition, rejection of all but the multi-opposition objects does not significantly change our results; as expected, the total number of KBOs estimated decreased by a factor ~ 2 and error bars increased by a factor $\sim \sqrt{2}$ due to the sample size reduction. The eccentricity and semimajor axes of all objects with $a < 50$ AU (this includes all Classical KBOs) appear in Figure 6.

In the next two sections, we use our observations to constrain three fundamental quantities of the Classical KBOs: (1) the size distribution index, q , (2) the half-width of

the inclination distribution, $i_{1/2}$, and (3) the total number of CKBOs larger than 100 km in diameter, $N_{\text{CKBOs}}(D > 100 \text{ km})$. The quantities $i_{1/2}$ and q are uncorrelated, as the observable constraining $i_{1/2}$ is the inclination distribution and the observable constraining q is the absolute magnitude distribution. However, $N_{\text{CKBOs}}(D > 100 \text{ km})$ is a function of both q and $i_{1/2}$ as a steeper size distribution or thicker inclination distribution will each allow more bodies to be present. In the maximum likelihood simulations that follow, the ideal case would be to constrain q , $i_{1/2}$ and $N_{\text{CKBOs}}(D > 100 \text{ km})$ and estimate errors in one simulation, however, this is difficult computationally. Therefore, we find the best-fit values of the three parameters in a single simulation, but estimate the errors on the parameters in two simulations, one that estimates the q - $N_{\text{CKBOs}}(D > 100 \text{ km})$ joint errors and one that estimates the $i_{1/2}$ - $N_{\text{CKBOs}}(D > 100 \text{ km})$ joint errors. We then combine the two simulation results in quadrature to determine the errors on $N_{\text{CKBOs}}(D > 100 \text{ km})$.

3. The Size Distribution of the Classical KBOs

We estimate the size distribution of the KBOs from our data in two ways. The first is a simple estimate made directly from the distribution of ecliptic KBO apparent magnitudes (CLF). The second is a model which simulates the discovery characteristics of our survey through the use of a maximum likelihood model constrained by the absolute magnitude of the Classical KBOs.

3.1. Cumulative Luminosity Function

We model the CLF with a power-law relation, $\log \Sigma = \alpha(m_R - m_0)$ (§1). The KBOs are assumed to follow a differential power-law size distribution of the form $n(r)dr \propto r^{-q}dr$, where $n(r)dr$ is the number of objects having radii between r and $r + dr$, and q is the index of the size distribution. Assuming albedo and heliocentric distance distributions that are independent of KBO size, the simple transformation between the slope of the CLF (α) and the exponent of the size distribution (q) is given by (Irwin et al. 1995),

$$q = 5\alpha + 1. \quad (3)$$

Under these assumptions, the size distribution can be estimated directly from the CLF.

We estimated the CLF by multiplying the detection statistics from the observed distribution of object brightnesses by the inverse of the detection efficiency. We assumed Poisson detection statistics, with error bars indicating the interval over which the integrated Poisson probability distribution for the observed number of objects contains 68.27% of

the total probability (identical to the errors derived by Kraft, Burrows & Nousek 1991). This is nearly equal to the Gaussian case for all data points resulting from more than a few detections. We have included all 74 KBOs discovered in our 37.2 sq deg of ecliptic fields in the estimate of the CLF. This includes the lost objects, as the CLF is simply a count of the number of bodies discovered at a given apparent magnitude. Our results appear in Figure 7, with other published KBO surveys. All observations were converted to R -band if necessary assuming $V - R = 0.5$ for KBOs (Luu & Jewitt 1996), and error bars were computed assuming Poisson detection statistics. The data point of Cochran et al. (1995) near $m_R = 28$ was omitted because of major uncertainties about its reliability (Brown, Kulkarni & Liggett 1997, cf. Cochran et al. 1998). Early photographic plate surveys (Tombaugh 1961, portions of Luu & Jewitt 1988, and Kowal 1989) have unproven reliability at detecting faint slow-moving objects, and plate emulsion variations and defects make accurate photometric calibration difficult. The photographic plate survey data were not used in our analysis.

The CLF points are highly correlated with one another, resulting in a heavy weighting of the bright object data points. Thus, we fitted the Differential Luminosity Function (DLF) instead. We plot the DLF data points at the faint end of the bin, representing the modal value in that bin. Very small bin sizes were chosen (0.1 magnitudes) to negate binning effects incurred from averaging the detection efficiency (Equation 2) over a large magnitude range. For any non-zero CLF slope, α , the DLF and CLF slopes are equal due to the exponential nature of the CLF. The DLF was modelled by evaluating the Poisson probability of detecting the observed DLF given a range of m_0 and α , with the maximum probability corresponding to our best-fit values. Error bars were determined by finding the contours of constant joint probability for m_0 and α enclosing 68.27% of the total probability, a procedure similar to that used below for the maximum likelihood simulation. Computations from this procedure are summarized in Table 7. We find that the slope of the CLF is $\alpha = 0.64^{+0.11}_{-0.10}$ with $m_0 = 23.23^{+0.15}_{-0.20}$, which corresponds to $q = 4.2 \pm 0.5$ from Equation 3. We also fitted the CLF by applying the maximum likelihood method described by Gladman et al. (1998) to our data, which yields statistically identical results to the binned DLF procedure: $\alpha = 0.63 \pm 0.06$ and $m_0 = 23.04^{+0.08}_{-0.09}$, corresponding to $q = 4.2 \pm 0.3$. The maximum-likelihood method provides slightly better signal-to-noise, and is independent of binning effects. However, it does not provide a visualization of the data, as presented for the DLF fit. We adopt the maximum-likelihood procedure as our formal estimate of the CLF slope. Both methods estimating the size distribution are in statistical agreement with the more detailed analysis presented in the next section.

The best-fit $\alpha = 0.63$ magnitude distribution was compared with the observed magnitude distribution using a Kolmogorov-Smirnov test (Press et al. 1992), producing

a value of $D = 0.13$. If the model and the data distributions were identical, a deviation greater than this would occur by chance 12% of the time. Thus, our linear model is not a perfect fit, but it is statistically acceptable.

3.2. Maximum Likelihood Simulation

We now present more detailed analysis of the size distribution. Since we model the detection statistics of an assumed population, we choose to model the 49 Classical KBOs discovered on the ecliptic as they are numerically dominant in the observations and their orbital parameters are more easily modelled than other KBO classes. Our selection criteria for CKBOs are perihelion $q' > 37$ AU and $40.5 \text{ AU} < a < 46 \text{ AU}$. Given the size of an object and its orbital parameters, we can compute its position, velocity, and brightness, allowing a full “Monte-Carlo” style analysis of the bias effects of our data collection procedures. The apparent brightness was computed from:

$$m = m_{\odot} - 2.5 \log(p\Phi(\alpha')r^2) + 2.5 \log(2.25 \times 10^{16} R^2 \Delta^2), \quad (4)$$

where α' is the phase angle of the object, $\Phi(\alpha')$ is the *Bowell et al. (1989)* phase function, geometric albedo is given by p , r is the object radius in kilometers, R is the heliocentric distance, and Δ is the geocentric distance, both in AU (*Jewitt & Luu 1995*). The apparent red magnitude of the Sun was taken to be $m_{\odot} = -27.1$. For this work, we assume $p = 0.04$, consistent with a Centaur-like albedo (*Jewitt & Luu 2000*). We neglect phase effects (setting $\Phi(\alpha') \equiv 1$) since the maximum phase angle of an object at $R = 40$ AU within 1.5 hours of opposition is $\alpha' = 0.55^\circ$. This corresponds to $\Phi(\alpha') = 0.91$, a change in brightness of only 0.09 magnitudes, which is less than other uncertainties in the data.

This apparent brightness is used in a biasing-correction procedure (*Trujillo, Jewitt & Luu 2000* and *Trujillo 2000*), summarized here:

1. A model distribution of KBOs is assumed (described in Table 8).
2. KBOs are drawn randomly from the model distribution.
3. For each KBO, the apparent speed and ecliptic coordinates are computed from the equations of *Sykes & Moynihan (1996*, a sign error was found in Equation 2 of their text and corrected), and compared to the observed fields and speed criteria.
4. The apparent magnitude is computed from Equation 4.
5. The efficiency function (Equation 2) and our field area covered are used to determine if the simulated object would be “detected” in our survey.

6. A histogram of the detection statistics for the simulated objects is constructed, logarithmically binned by object size for the size distribution model and binned by inclination for the inclination-distribution model. Binning effects were negligible due to small bin choice.
7. Steps 1-6 are repeated until the number of detected simulated objects is at least a factor 10 greater than the number of observed objects in each histogram bin (typically requiring a sample of $10^6 < N < 10^8$ simulated objects, depending on the observed distribution).
8. The likelihood of producing the observed population from the model is estimated by assuming that Poisson detection statistics ($P = \frac{\mu^n}{n!} \exp(-\mu)$) apply to each histogram bin, where μ represents the expected number of simulated objects “discovered” given the number of objects simulated and n represents the true number of KBOs observed. Thus, the observed size distribution, calculated from Equation 4, is used to constrain the q model, and the observed inclination distribution is used to constrain the i model (§ 4).

These steps are repeated for each set of model parameters in order to estimate the likelihood of producing the observations for a variety of models.

For the size distribution analysis, we take our best-fit model of the width of the inclination distribution (Half-Width $i_{1/2} = 20^\circ$, as estimated in the next section), and vary the size distribution index q , and the total number of objects $N_{\text{CKBOs}}(D > 100 \text{ km})$. Model parameters are summarized in Table 8 and results appear in Figure 8. Our best-fit values are

$$\begin{aligned}
 q &= 4.0^{+0.6}_{-0.5} & (1\sigma) \text{ and} \\
 &= 4.0^{+1.3}_{-2.1} & (3\sigma), \\
 &\text{and} \\
 N_{\text{CKBOs}}(D > 100 \text{ km}) &= 3.8^{+2.0}_{-1.5} \times 10^4 & (1\sigma) \text{ and} \\
 &= 3.8^{+5.4}_{-2.7} \times 10^4 & (3\sigma),
 \end{aligned}$$

where the errors for $N_{\text{CKBOs}}(D > 100 \text{ km})$ have been combined in quadrature from the results of the q and $i_{1/2}$ fits, as described at the end of § 2.1. The values for q are consistent with previously published works (Table 9) and the q derived from the CLF data in the simple model (Equation 3). The results are consistent with the distribution of large ($D > 150 \text{ km}$) main-belt asteroids ($q = 4.0$, Cellino, Zappalá, & Farinella 1991) and rock crushed by hypervelocity impacts ($q = 3.4$, Dohnanyi 1969). In addition, the scenario where the cross-sectional area (and thus optical scattered light and thermal emission) is concentrated in the largest objects ($q < 3$, Dohnanyi 1969) is ruled out at the $> 2\sigma$

(> 95.4% confidence) level. Our results are also consistent with Kenyon & Luu (1999) who simulate the growth and velocity evolution of the Kuiper Belt during the formation era in the Solar System. They find several plausible models for the resulting size distribution, all of which have $q \approx 4$. In Figure 9 we plot the best-fit model CKBO distribution with the observed DLF to demonstrate the expected results from different size distributions.

The magnitude distribution expected from the maximum likelihood model was compared to the observed magnitude distribution, as was done for the CLF-derived magnitude distribution in § 3.1. The Kolmogorov-Smirnov test produced $D = 0.17$; a greater deviation would occur by chance 11% of the time.

In our Classical KBO maximum likelihood simulation, we have ignored possible contributions of the 7 lost KBOs, since their orbital classes are not known. However, including them in the simulations by assuming circular orbits at the heliocentric distance of discovery results in statistically identical results for q , and the expected 7/49 rise in $N_{\text{CKBOs}}(D > 100 \text{ km})$.

4. Inclination Distribution of the Classical KBOs

The dynamical excitation of the Kuiper Belt is directly related to the inclination distribution of the KBOs. We present the inclinations of the CKBOs found in the CFHT survey in Figure 10. Assuming heliocentric observations, a KBO in circular orbit follows

$$\sin \beta = \sin i \sin f \quad (5)$$

where β is the heliocentric ecliptic latitude, $0 < i < 90^\circ$ is the inclination, and $0 < f < 360^\circ$ represents the true anomaly of the object’s orbit with $f = 0$ and 180° representing the ecliptic plane crossing (the longitude of perihelion is defined as 0 in this case). Using Equation 5, we plot the fraction of each orbit spent at various ecliptic latitudes as a function of i (Figure 11). This plot demonstrates two trends concerning the ecliptic latitude of observations β_{obs} . First, high-inclination objects are a factor 3–4 times more likely to be discovered when $\beta_{\text{obs}} \sim i$ than when observing at low ecliptic latitudes ($\beta_{\text{obs}} < i$). Second, the number of expected high-inclination objects drops precipitously, roughly as $1/i$, once $i > 1.5\beta_{\text{obs}}$ (Jewitt, Luu & Chen 1996).

These facts led us to observe at three different ecliptic latitudes (0° , 10° and 20°) to better sample the high-inclination objects. During two observation periods (Sep 1999 and Mar 2000) care was made to interleave the ecliptic fields with the off-ecliptic fields on timescales of ~ 30 minutes. This technique provides immunity to drift in the limiting magnitude which might otherwise occur in response to typical slow changes in the seeing

through the night. The results for the robust, interleaved fields matched those for the seeing-corrected Feb 1999 fields where fields were interleaved on much longer timescales of ~ 3 hours. Accordingly, we combined the data sets from all epochs to improve signal-to-noise. In the next sections, we analyse the inclination distribution using two techniques to demonstrate the robustness of our method.

4.1. Simple Inclination Model

First, since fields were imaged at three different ecliptic latitudes, the surface density of objects at each latitude band ($\Sigma(0^\circ)$, $\Sigma(10^\circ)$ and $\Sigma(20^\circ)$) can directly yield the underlying inclination distribution. In our simple model, we generate an ensemble of inclined, circular orbits drawn from a Gaussian distribution centered on the ecliptic, and having a characteristic Half-Width of $i_{1/2}$. The probability of drawing a KBO with inclination between i and $i + di$ is given by

$$P(i)di = \frac{1}{\sigma\sqrt{2\pi}} \exp\left(\frac{-i^2}{2\sigma^2}\right) di, \quad (6)$$

where $\sigma = i_{1/2}/\sqrt{2\ln 2}$. Using this relation, and Equation 5, we simulate the expected values of $\Sigma(0^\circ)$, $\Sigma(10^\circ)$ and $\Sigma(20^\circ)$ for various $i_{1/2}$. These are compared to two ratios measured from our observations, $R(10^\circ, 0^\circ) \equiv \Sigma(10^\circ)/\Sigma(0^\circ)$ and $R(20^\circ, 0^\circ) \equiv \Sigma(20^\circ)/\Sigma(0^\circ)$. Results appear in Table 10, and demonstrate that the characteristic half-width of the inclination distribution in the Kuiper Belt is $i_{1/2} \sim 17^{+10}_{-4}^\circ$ ($1\sigma = 68.27\%$ confidence). This simple model does not use the observed inclination distribution of the individual objects, merely the surface density of objects found at each ecliptic latitude, thus we have combined all objects from all KBO classes into this estimate.

4.2. Full Maximum Likelihood Inclination Model

Second, we use the maximum likelihood model described in §3.1. We list the parameters of the model in Table 11. This model encompasses the additional constraint of the observed inclination distribution, as well as the parallactic motion of the Earth and KBO orbital motion to produce more realistic results. Results appear in Figure 12, with $N_{\text{CKBOs}}(D > 100 \text{ km})$ representing the number of CKBOs with diameters greater than 100

km. The maximum likelihood occurs at

$$\begin{aligned}
 i_{1/2} &= 20^{+6}_{-4}{}^{\circ} & (1\sigma) \text{ and} \\
 &= 20^{+26}_{-8}{}^{\circ} & (3\sigma), \\
 &\text{and} \\
 N_{\text{CKBOs}}(D > 100 \text{ km}) &= 3.8^{+2.0}_{-1.5} \times 10^4 & (1\sigma) \text{ and} \\
 &= 3.8^{+5.4}_{-2.7} \times 10^4 & (3\sigma),
 \end{aligned}$$

where the errors for $N_{\text{CKBOs}}(D > 100 \text{ km})$ have been estimated from the $i_{1/2}$ and q fits, combined in quadrature, as described at the end of § 2.1. This maximum likelihood model is consistent with the simple model described in §4.1. In Figure 13, we plot the observed surface density of objects as a function of ecliptic latitude and compare these data to our best-fit models. This illustrates the fundamental fact that even though the true inclination distribution of the KBOs is very thick ($i_{1/2} \approx 20^\circ$), the surface density drops off quickly with ecliptic latitude, reaching half the ecliptic value at an ecliptic latitude of $\beta \approx 3^\circ$ ($\Sigma(3^\circ)/\Sigma(0^\circ) < 0.5$).

The functional form of the inclination distribution cannot be well constrained by our data. However, the best-fit Gaussian distribution was compared to a flat-top (“top-hat”) inclination distribution, with a uniform number of objects in the $0^\circ < i < 30^\circ$ range. The Gaussian and flat-top models were equally likely to produce the observed distribution in the 65% confidence limit ($< 1\sigma$). A Gaussian model multiplied by $\sin(i)$ was also tried but could be rejected at the $> 3\sigma$ level because it produced too few low-inclination objects. We also tested the best-fit model presented by Brown (2001), consisting of two Gaussians multiplied by $\sin(i)$,

$$\left[a \exp\left(\frac{-i^2}{2\sigma_1^2}\right) + (1 - a) \exp\left(\frac{-i^2}{2\sigma_2^2}\right) \right] \sin i, \quad (7)$$

where $a = 0.93$, $\sigma_1 = 2.2^\circ$, and $\sigma_2 = 18^\circ$, and found it equally compatible with our single Gaussian model (Equation 6). Because the Gaussian model was the simplest model that fit the observed data well, we chose it to derive the following velocity dispersion results.

We first find the mean velocity vector of all the simulated best-fit CKBOs, \vec{v} , in cylindrical coordinates (normal vectors \hat{r} , $\hat{\theta}$, and \hat{z} representing the radial, longitudinal and vertical components respectively). The mean velocity vector \vec{v} is consistent with a simple Keplerian rotation model at $R \approx 46 \text{ AU}$. We then compute the relative velocity of each KBO from this via $|\vec{v} - \vec{v}_i|$, where \vec{v}_i is the velocity dispersion contribution of the i th KBO. We find the resulting root-mean-square (RMS) velocity dispersion of the \hat{r} , $\hat{\theta}$, and \hat{z} components to be equal to $\Delta v_r = 0.51 \text{ km/s}$, $\Delta v_\theta = 0.50 \text{ km/s}$, and $\Delta v_z = 0.91 \text{ km/s}$, combining in quadrature for a total velocity dispersion of $\Delta v = \sqrt{\Delta v_r^2 + \Delta v_\theta^2 + \Delta v_z^2} = 1.16$

km/s. An error estimate of the velocity dispersion can be found by following a similar procedure for the $i_{1/2} = 16^\circ$ and $26^\circ (\pm 1\sigma)$ models, yielding $\Delta v = 1.16^{+0.25}_{-0.16}$ km/s.

4.3. Inferred Mass

The Kuiper Belt mass inferred from these results can be directly calculated from the size distribution and the number of bodies present. For the best-fit $q = 4.0$ size distribution, the mass of CKBOs in bodies with diameters $D_{\min} < D < D_{\max}$ is

$$M(D_{\min}, D_{\max}) = \frac{4}{3} \pi \rho \Gamma \ln(D_{\max}/D_{\min}), \quad (8)$$

where ρ is the bulk density of the object. The normalization constant Γ is calculated from the results of our simulation,

$$\Gamma \approx 3.0 \times 10^{12} \text{ m}^3 p_R^{-1.5} N(D > 100 \text{ km}), \quad (9)$$

where $N(D > 100 \text{ km}) = 3.8 \times 10^4$ (§4.2), yielding $\Gamma = 1.4 \times 10^{19} \text{ m}^3$ assuming $p_R \equiv 0.04$. The mass for $100 \text{ km} < D < 2000 \text{ km}$ then becomes

$$M(100 \text{ km}, 2000 \text{ km}) \approx 0.03 M_{\oplus} \left(\frac{\rho}{1000 \text{ kg m}^{-3}} \right) \left(\frac{0.04}{p_R} \right)^{1.5}, \quad (10)$$

where $M_{\oplus} = 6.0 \times 10^{24} \text{ kg}$ is the mass of the earth. The uncertainties on this value are considerable as the characteristic albedo and density of the CKBOs are unknown.

4.4. Comparison of the Classical KBOs to Other Dynamical Classes

We found that the total number of CKBOs is given by $N_{\text{CKBOs}}(D > 100 \text{ km}) = 3.8^{+2.0}_{-1.5} \times 10^4$. This can be compared to the other main dynamical populations (the Resonant and Scattered KBOs) from our data. Observational biases favor the detection of the Plutinos over the Classical KBOs due to their closer perihelion distance. We found only 7 Plutinos (4 ecliptic and 3 off-ecliptic) so we can make only crude (factor ~ 2 statements) about the true size of the population. Thus, we use the results of Jewitt, Luu & Trujillo (1998) who estimate that the apparent fraction of Plutinos (P_a) in the Kuiper Belt is enhanced relative to the intrinsic fraction (P_i) by a factor $P_a/P_i \approx 2$ for $q = 4.0$ and $r_{\max} = 1000 \text{ km}$. Applying this correction to our ecliptic observations (4 Plutinos and 49 Classical KBOs) indicates that the total number of Plutinos larger than 100 km in diameter is quite small,

$$N_{\text{Plutinos}}(D > 100 \text{ km}) \approx \frac{4}{4 + 49} \frac{P_i}{P_a} N_{\text{CKBOs}} \approx 1400. \quad (11)$$

The populations of the Plutinos and the 2:1 Resonant objects are important measures of the resonance sweeping hypothesis (Malhotra 1995), which predicts equal numbers of objects in each resonance. Since the 2:1 objects are systematically farther from the sun than the Plutinos, the true Plutino/2:1 ratio is higher than the observed ratio. Jewitt, Luu & Trujillo (2000) estimate the observed/true bias correction factor to be ≈ 0.310 for a survey similar to ours ($q = 4$ and $m_{R50} = 24.0$). Only 2 of our objects (both found on the ecliptic) are < 0.5 AU from the 2:1 Resonance, so we find the Plutino/2:1 fraction is given by $(4/2)0.310 \approx 0.6$. Due to the small number of bodies involved, this is only an order of magnitude estimate. Within the uncertainties, our observations are consistent with the hypothesis that the 3:2 and 2:1 resonances are equally populated.

The observational biases against the Scattered KBOs are considerable. Trujillo, Jewitt & Luu (2000) estimate the total population of the Scattered KBOs to be $N_{\text{SKBOs}}(D > 100 \text{ km}) = 3.1^{+1.9}_{-1.3} \times 10^4$, approximately equal to the population of Classical KBOs derived from our data. We summarize the relative populations by presenting their number ratios:

$$\text{Classical} : \text{Scattered} : \text{Plutino} : \text{Resonant 2:1} = 1.0 : 0.8 : 0.04 : 0.07. \quad (12)$$

5. The Edge of the Classical Kuiper Belt

We found no objects beyond heliocentric distance $R_{\text{obs}} = 48.9$ AU. There are two possibilities to explain this observation: (1) this is an observational bias effect and the bodies beyond R_{obs} cannot be detected in our survey, or (2) there is a real change in the physical or dynamical properties of the KBOs beyond R_{obs} . In order to test these two possibilities, we compare the expected discovery distance of an untruncated Classical Kuiper Belt to the observations, as depicted in Figure 14. This untruncated CKBO distribution is identical to our best-fit model from § 4.2, except $40.5 \text{ AU} < a < 200 \text{ AU}$, instead of $40.5 \text{ AU} < a < 46 \text{ AU}$. The total number of bodies produced was considered a free parameter in this model. Inspecting Figure 14, the absence of detections beyond 50 AU is inconsistent with an untruncated model with R^{-2} radial power to the ecliptic plane surface density. Assuming Poisson statistics apply to our null detection beyond R_{max} , the 99.73% (3σ) upper limit to the number of bodies (μ) expected beyond R_{max} can be calculated from $1 - 0.9973 = \exp(-\mu)$, yielding $\mu = 5.9$ KBOs. We found 49 ecliptic Classical KBOs inside the R_{max} limit, so the 3σ upper limit to the number density of KBOs beyond R_{max} is $49/5.9 \approx 8$ times less than the number density of Classical KBOs. Although we have constrained the outer edge by the heliocentric distance at discovery R , which is a directly observable quantity, a dynamical edge would be set by the semimajor axes (a) of the object

orbits. This difference has little effect on our findings as the known CKBOs occupy nearly circular orbits with median eccentricity $e = 0.08$ (the calculated median is conservative as it includes only bodies with $e > 0$ to protect against short-arc orbits, which typically assume $e = 0$). Since an untruncated distribution (1) is incompatible with our data, we must conclude that scenario (2) applies — there must be a physical or dynamical change in the KBOs beyond R_{\max} .

There are several possible physical and dynamical mechanisms that could produce the observed truncation of the belt beyond $R_{\max} = 50$ AU (Jewitt, Luu & Trujillo 1998): (1) the size distribution of the belt might become much steeper beyond R_{\max} , putting most of the mass of the belt in the smallest, undetectable objects; (2) the size distribution could be the same ($q = 4$), but there might be a dearth of large (i.e. bright) objects beyond R_{\max} , suggesting prematurely arrested growth; (3) the objects beyond R_{\max} may be much darker and therefore remain undetected; (4) the eccentricity distribution could be lower in the outer belt, resulting in the detection of fewer bodies; (5) the ecliptic plane surface density variation with radial distance may be steeper than our assumed $p = 2$; and (6) there is a real drop in the number density of objects beyond R_{\max} . We consider each of these cases in turn, and their possible causes.

Detailed simulations of the growth of planetesimals in the outer Solar System have not estimated the radial dependence of the formation timescale (e.g. Kenyon & Luu 1999). However, it is expected that growth timescales should increase rapidly with heliocentric distance, perhaps as $t \propto R^3$ (Wetherill 1989). One could then expect a reduction in the number of large objects beyond 50 AU, as per (2) above, and a correspondingly steeper size distribution, as in (1), at larger heliocentric distances. However, with $t \propto R^3$, the timescales for growth at $R = 41$ AU (inner edge) and $R = 50$ AU (outer edge) are only in the ratio 1.8:1. In addition, we observe no correlation between size and semimajor axis among the Classical KBOs.

To test scenario (1), we took our untruncated best-fit model and varied the size distribution index q_{out} for bodies with semimajor axes $a > R_{\max}$, keeping the KBO mass across the R_{\max} boundary constant. We then found the minimum q_{out} consistent with our null detection beyond R_{\max} . This mass-conservation model is very sensitive to the chosen minimum body radius r_{\min} , because for any $q_{\text{out}} > 4$, most of the mass is in the smallest bodies (Dohnanyi 1969). The minimum size-distribution index required as a function of r_{\min} appears in Table 12. If mass is conserved for the observable range of bodies, $r_{\min} = 50$ km, the observed edge cannot be explained by a change in the size distribution unless $q > 10$ (3σ), an unphysically large value. For the conservative case of $r_{\min} = 6$ km (roughly the size of cometary nuclei, Jewitt 1997), the observed edge could only be explained by

$q > 5.6$ (3σ) beyond R_{\max} . We know of no population of bodies with a comparably steep size distribution. Thus, we conclude that the observed edge is unlikely to be solely caused by a change in the size distribution beyond R_{\max} .

A similar procedure was followed for possibility (2). Here again, we took our best-fit truncated model and extended it to large heliocentric distances. Then, r_{\max} was varied to find the largest value that could explain our null detection beyond R_{\max} , keeping the total number density of objects with radii $r < r_{\max}$ constant. We found that $r_{\max} < 75$ km (3σ) was required beyond R_{\max} to explain the observed edge. This is a factor ~ 5 smaller radius and a factor ~ 150 less volume than our largest object found within R_{\max} (1999 CD₁₅₈, ~ 400 km in radius). Such a severe change in the maximum object size beyond R_{obs} would have to occur despite the fact that growth timescales vary by less than a factor of ~ 2 over the observed Classical KBO range, as explained above.

One might also expect (3) to be true, as KBO surfaces could darken over time with occasional resurfacing by collisions (Luu & Jewitt 1996), and long growth timescales indicate long collision timescales as well. However, the geometric albedo would have to be $p < 0.008$, a factor 5 lower than that of the CKBOs in our model, assuming a constant number density of objects across the transition region. We are not aware of natural planetary materials with such low albedos.

The dynamical cases (4), a drop in the eccentricity distribution, and (5), a steeper ecliptic plane density index, can also be rejected. Even an extreme change in the eccentricity distribution cannot explain our observations. Lowering eccentricity from $e = 0.15$ (a high value for the Classical KBOs) to $e = 0$ results in a perihelion change from 42.5 AU to 50 AU for an object with semimajor axis 50 AU. Such a change corresponds to a 0.7 magnitude change in perihelion brightness, and to a factor 2.8 change in the surface density of objects expected from our $\alpha = 0.63$ CLF. This model is rejected by our observations at the $> 5\sigma$ level. The variation in ecliptic plane surface density with respect to heliocentric distance was assumed to follow a power law with index $p = 2$ in our model. However, even a large increase to $p = 5$ would result in a reduction in surface density of a factor 2.7 in the 41 AU to 50 AU range, which can also be rejected as the cause of our observed edge at the $> 5\sigma$ level.

Since scenarios (1) through (5) seem implausible at best, we conclude that the most probable explanation for the lack of objects discovered beyond R_{\max} is (6), the existence of a real, physical decrease in object number density. There have been few works considering mechanisms for such truncation. The 2:1 mean-motion Neptune resonance at $a \sim 47.8$ AU is quite close to the observed outer edge of the belt. However, given the Neptune resonance sweeping model (Malhotra 1995), the resonance could not cause an edge. The sweeping

theory predicts that the 2:1 resonance should have passed through the Classical Kuiper Belt as Neptune’s orbit migrated outwards to its present semimajor axis. Thus, the KBOs interior to the current 2:1 resonance ($a \approx 47.8$ AU) could have been affected by this process, but an edge at R_{max} cannot be explained by such a model. Ida, Larwood & Burkert (2000) simulate the effect of a close stellar encounter on the Kuiper Belt, suggesting that KBO orbits beyond 0.25–0.3 times the stellar perihelion distance would be disrupted and ejected for a variety of encounter inclinations. Thus, an encounter with a solar mass star with perihelion at ~ 200 AU might explain the observed edge. Such encounters are implausible in the present solar environment but might have been more common if the sun formed with other stars in a dense cluster.

6. Constraints on a Distant Primordial Kuiper Belt

While our observations indicate a dearth of objects beyond 50 AU, it is also possible that a “wall” of enhanced number density exists at some large $R \gtrsim 100$ AU distance, as suggested by Stern (1995). We know that the Kuiper Belt has lost much mass since formation because the present mass is too small to allow the observed objects to grow in the age of the solar system. Kenyon & Luu (1999) found that the primordial Kuiper Belt mass in the $30 \text{ AU} < R < 50 \text{ AU}$ region could have been some $\sim 10M_{\oplus}$, compared to the $\sim 0.1M_{\oplus}$ we see today. Stern (1995) also speculated that the primordial surface density may be present at large heliocentric distances. We model this primordial belt as analogous to the CKBOs in terms of eccentricity, inclination and size distribution, but containing a factor of 100 more objects and mass per unit volume of space. These objects would be readily distinguishable from the rest of the objects in our sample as they would have low eccentricities characteristic of the CKBOs ($e < 0.25$) yet would have very large semimajor axes ($a > 90$ AU). Since we have discovered no such “primordial” objects, Poisson statistics state that the 3σ upper limit to the sky-area number density of primordial KBOs is 5.9 in 37.2 sq deg, or $0.16 \text{ primordial KBOs deg}^{-2}$. We constrain the primordial KBOs by allowing the inner edge of the population, a_{min} , to vary outwards, while keeping the outer edge fixed at 250 AU. We find that $a_{\text{min}} = 130$ AU coincides with the 3σ limit on the inner edge of the belt, nearly at the extreme distance limit of our survey. An object discovered at our survey magnitude limit $m_{R50} = 23.7$ at this distance would have diameter $D \approx 1800$ km (approximately 25% smaller than Pluto) assuming a 4% albedo.

7. Summary

New measurements of the Kuiper Belt using the world’s largest CCD mosaic array provide the following results in the context of our Classical KBO model.

(1) The slope of the differential size distribution, assumed to be a power law, is $q = 4.0^{+0.6}_{-0.5}$ (1σ). This is consistent with accretion models of the Kuiper Belt (Kenyon & Luu 1999). This distribution implies that the surface area, the corresponding optical reflected light and thermal emission are dominated by the smallest bodies.

(2) The Classical KBOs inhabit a thick disk with Half-Width $20^{+6}_{-4}^\circ$ (1σ).

(3) The Classical KBOs have a velocity dispersion of $1.16^{+0.25}_{-0.16}$ km/s.

(4) The population of Classical KBOs larger than 100 km in diameter $N_{\text{CKBOs}}(D > 100 \text{ km}) = 3.8^{+2.0}_{-1.5} \times 10^4$ (1σ). The corresponding total mass of bodies with diameters between 100 km and 2000 km is $M(100 \text{ km}, 2000 \text{ km}) \sim 0.03M_\oplus$, assuming geometric red albedo $p_R \equiv 0.04$ and bulk density $\rho \equiv 1000 \text{ kg m}^{-3}$.

(5) The approximate population ratios of the Classical, Scattered, 3:2 Resonant (Plutinos) and 2:1 Resonant KBOs are 1.0:0.8:0.04:0.07.

(6) The Classical Kuiper Belt has an outer edge at $R = 50 \text{ AU}$. This edge is unlikely to be due to a change in the physical properties of the CKBOs (albedo, maximum object size, or size distribution). The edge is more likely a real, physical depletion in the number of bodies beyond $\sim 50 \text{ AU}$.

(7) There is no evidence of a primordial (factor 100 density increase) Kuiper Belt out to heliocentric distance $R = 130 \text{ AU}$.

We thank Dave Tholen and Brian Marsden for providing orbits and ephemerides. We appreciate the vital observational assistance provided by Scott Sheppard and his help with astrometric measurements. We thank David Woodworth, Ken Barton, Lisa Wells and Christian Viellet for help at the CFH telescope. We are grateful for the assistance of John Dvorak, Chris Merrick, Lance Amano, Paul DeGroot and Farren Herron-Thorpe at the University of Hawaii 2.2 m telescope. A NASA grant to DCJ provided financial support for this project.

REFERENCES

- Aarseth, S. J., Lin, D. N. C, Palmer, P. L. 1993, AJ, 403, 351
- Allen, R. L., Bernstein, G. M., & Malhotra, R. 2001, submitted to ApJ
- Bowell, E., Hapke, B., Domingue, D., Lumme, K., Peltoniemi, J., Harris, A. 1989, in *Asteroids II*, edited by R. Binzel, T. Gehrels, & M. Matthews (University of Arizona, Tucson). p. 524–556
- Brown, M. E. 2001, submitted to AJ
- Brown, M. E., Kulkarni, S. R. & Liggett, T. J. 1997, ApJ, 490, L119–L122
- Cellino, A., Zappalá, V., & Farinella, P. 1991, MNRAS, 253, 561
- Chiang, E. I. & Brown, M. E. 1999, AJ, 118, 1411 (99CB)
- Cochran, A. L., Levison, H. F., Stern, S. A., & Duncan, M. J. 1995, ApJ, 455, 342
- Cochran, A. L., Levison, H. F., Tambllyn, P., Stern, S. A., & Duncan, M. J. 1998, ApJ, 503, L89
- Cuillandre, J.-C., Luppino, G., Starr, B., Isani, S. 2000, in “Astronomical Telescopes and Instrumentation”, Proc. SPIE, 4008, 1010
- Dohnanyi, J. S. 1969, J. Geophys. Res., 74, 2531
- Dones, L. 1997, in *ASP Conf. Ser. 122 From Stardust to Planetesimals* (Y. J. Pendleton, A. G. G. M. Tielens, eds.), pp. 347–365
- Duncan, M. J., & Levison, H. F. 1997, Science, 276, 1670
- Gladman, B., Kavelaars, J. J., Nicholson, P. D., Lored, T. J., Burns, J. A. 1998, AJ, 116, 2042 (98GKNLB)
- Hahn, J. M. & Malhotra, R. 1999, AJ, 117, 3041
- Ida, S., Larwood, J., Burkert, A. 2000, ApJ, 528, 351
- Irwin, M., Tremaine, S., & Żytkow, A. N. 1995, AJ, 110, 3082 (95ITZ)
- Jewitt, D. 1997, Earth, Moon & Planets, 79, 35–53.
- Jewitt, D. & Luu, J. 1993, Nature, 362, 730

- Jewitt, D. C. & Luu, J. X. 1995, *AJ*, 109, 1867
- Jewitt, D. & Luu, J. 1997, in *From Stardust to Planetesimals* edited by Y. J. Pendleton & A. G. G. M. Tielens (ASP Conference Series, Vol. 122), p. 335–345
- Jewitt, D. & Luu, J. 2000, in *Protostars and Planets IV*, eds. V. Mannings, A. Boss & S. Russell, Univ. of Arizona Press, Tucson, pp. 1201–1229
- Jewitt, D., Luu, J., & Chen, J. 1996, *AJ*, 112, 1225 (96JLC)
- Jewitt, D., Luu, J., & Trujillo, C. 1998, *AJ*, 115, 2125 (98JLT)
- Kenyon, S. J. & Luu, J. X. 1998, *AJ*, 115, 2136
- Kenyon, S. J. & Luu, J. X. 1999, *AJ*, 118, 1101
- Kowal, C. 1989, *Icarus*, 77, 118 (89K)
- Kraft, R., Burrows, D., Nousek, J. A. 1991, *ApJ*, 374, 344
- Landolt, A. U. 1992, *AJ*, 104, 340
- Levison, H. & Duncan, M. 1990, *AJ*, 100, 1669 (90LD)
- Luu, J. X. & Jewitt, D. C. 1988, *AJ*, 95, 1256 (88LJ)
- Luu, J., & Jewitt, D. 1996, *AJ*, 112, 2310
- Luu, J. X & Jewitt, D. C. 1998, *ApJ*, 502, L91 (98LJ)
- Luu, J., Marsden, B. G., Jewitt, D., Trujillo, C. A., Hergenrother, C. W., Chen, J., & Offutt, W. B. 1997, *Nature*, 387, 573
- Malhotra, R. 1995, *AJ*, 110, 420
- Morbidelli, A. & Valsecchi, G. B. 1997, *Icarus*, 128, 464
- Petit, J.-M., Morbidelli, A., Valsecchi, Giovanni B. 1999, *Icarus*, 141, 367
- Sheppard, S. S., Jewitt, D. C., Trujillo, C. A., Brown, M. J. I., & Ashley, M. C. B. A. 2000, *AJ*, 120, 2687 (00SJTBA)
- Stern, S. A. 1995, *AJ*, 110, 856
- Sykes, M. V. & Moynihan, P. D. 1996, *Icarus*, 124, 399

- Tombaugh, C. 1961, in *Planets and Satellites* (G. Kuiper & B. Middlehurst, Eds.), pp. 12–30. University of Chicago, Chicago (61T)
- Trujillo, C. 2000, in *Minor Bodies in the Outer Solar System* (A. Fitzsimmons, D. Jewitt, & R. M. West, Eds.), pp. 109–115. Springer-Verlag, Berlin
- Trujillo, C. & Jewitt, D. 1998, AJ, 115, 1680 (98TJ)
- Trujillo, C., Jewitt, D., & Luu, J. 2000, ApJ, 529, L103.
- Wetherill, G. W. 1989, in *The Formation and Evolution of Planetary Systems*, H. A. Weaver, L. Danly (eds.) (Cambridge University Press, Cambridge) pp 1–30

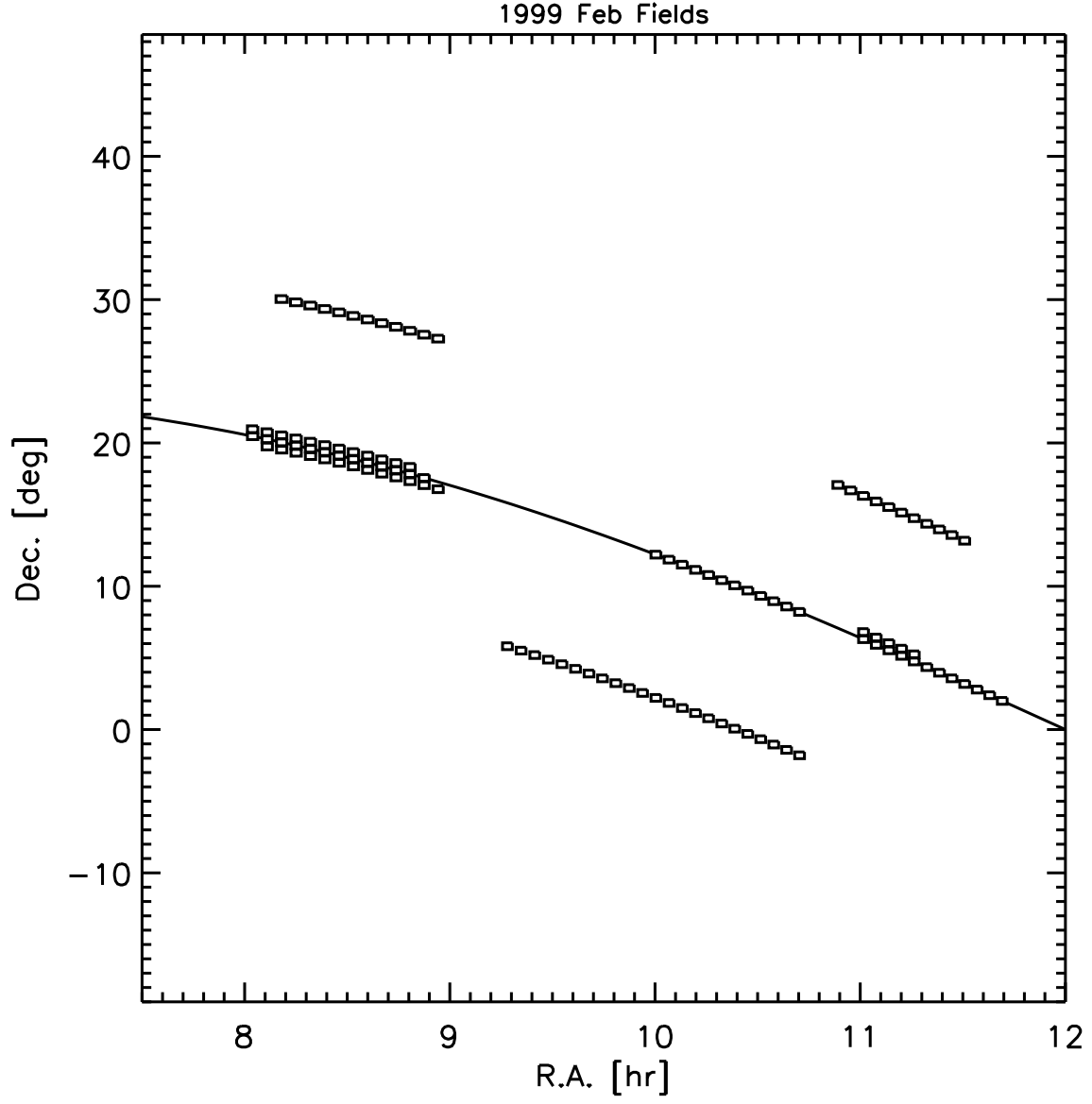


Fig. 1.— Fields imaged in Feb 1999. The ecliptic is denoted by a solid line.

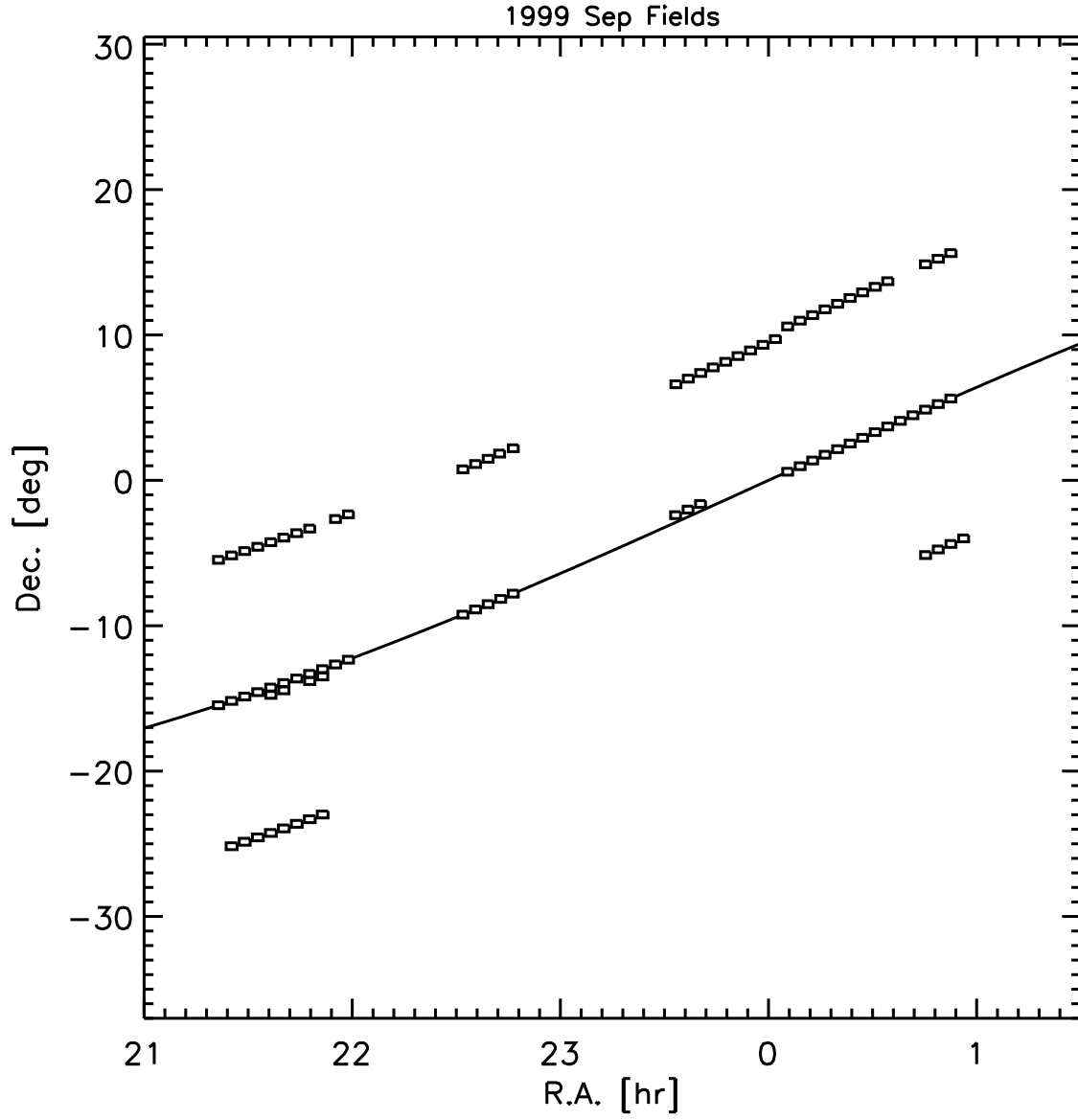


Fig. 2.— Fields imaged in Sep 1999. The ecliptic is denoted by a solid line.

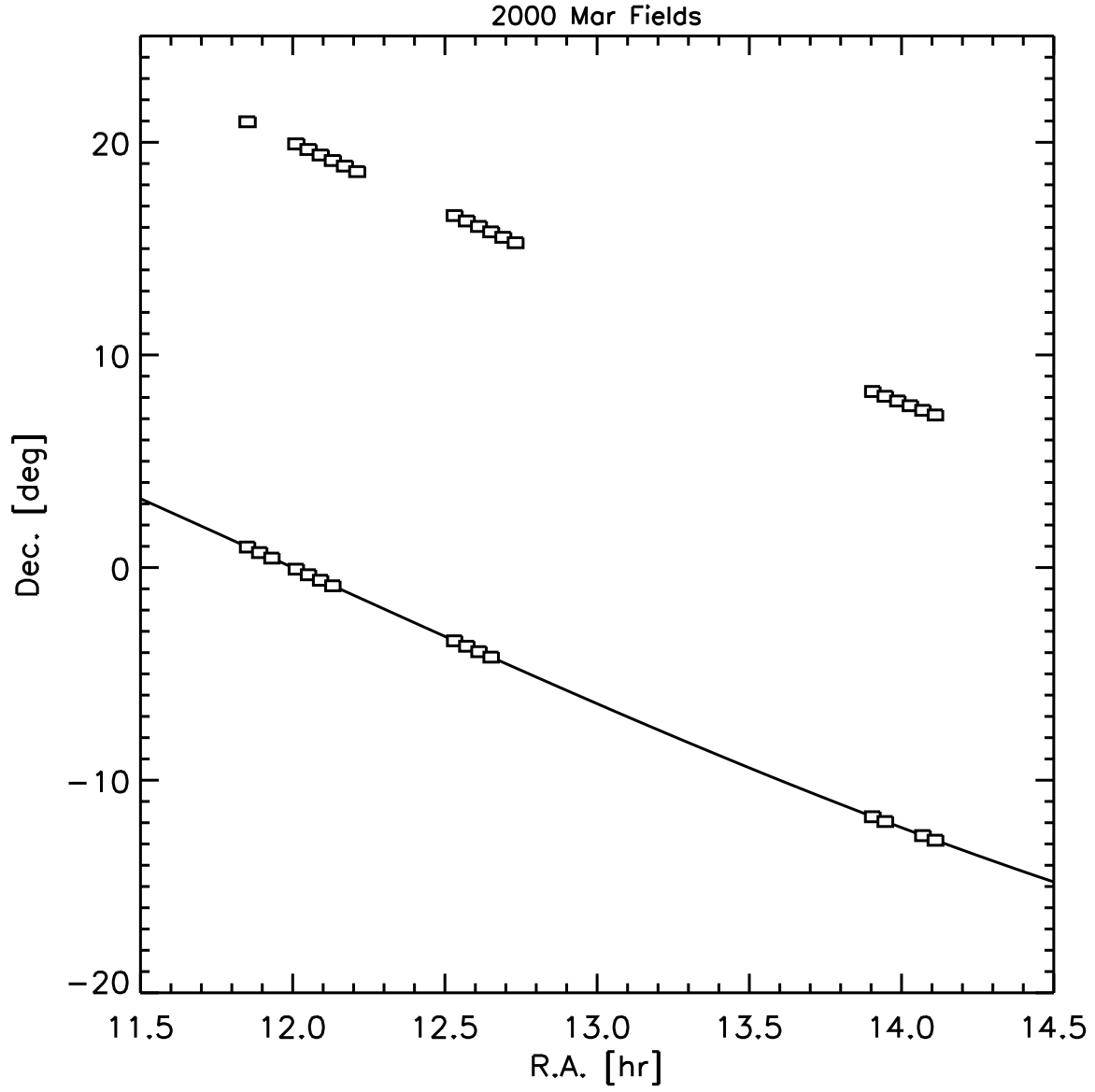


Fig. 3.— Fields imaged in Mar 2000. The ecliptic is denoted by a solid line.

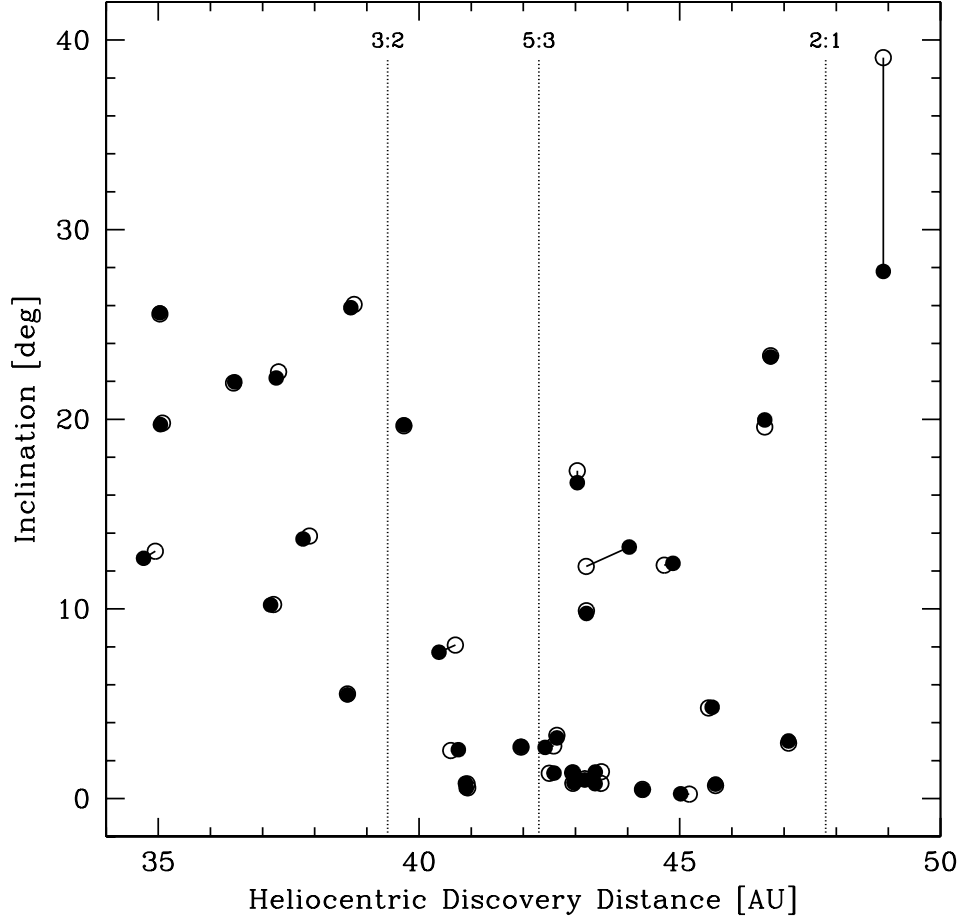


Fig. 4.— Inclination vs. discovery distance of all multi-opposition KBOs. The hollow circles represent quantities determined from < 90 day timebase during the first opposition. The connected filled circles represent the orbital solution including second opposition observations. Note that for all objects except one, quantities are well determined during the first opposition.

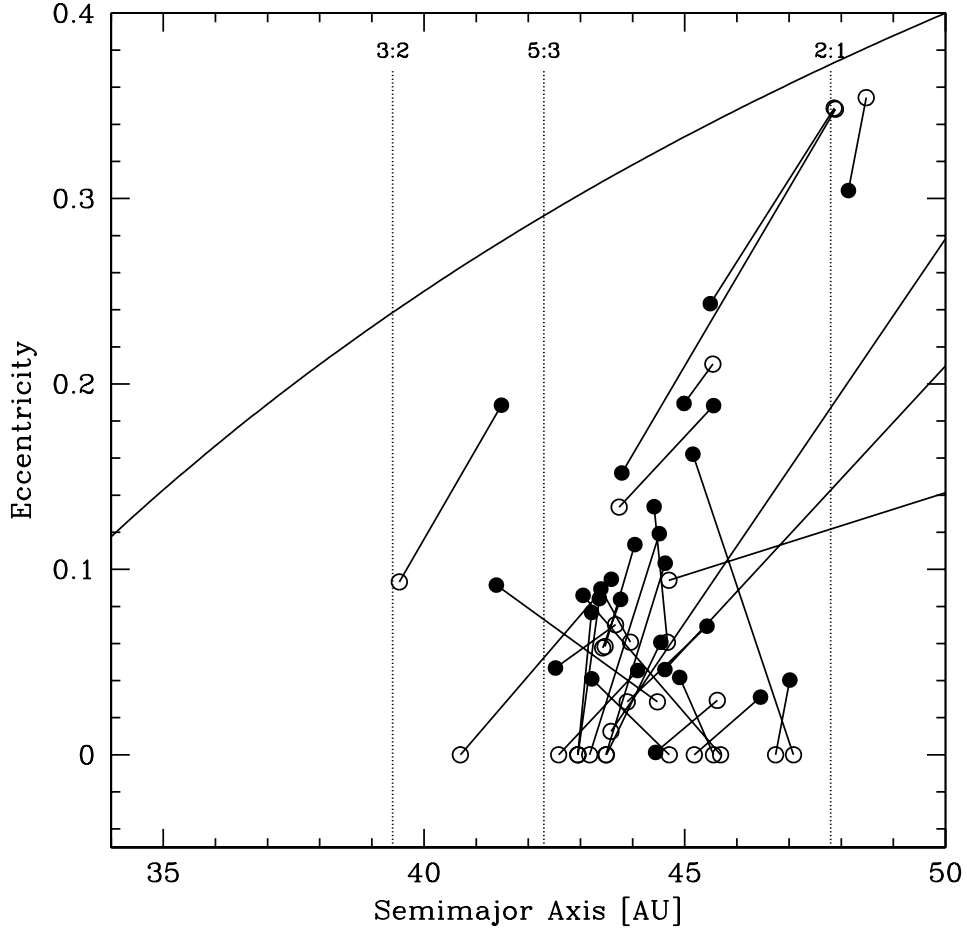


Fig. 5.— Eccentricity vs. semimajor axis of all multi-opposition KBOs with $a < 50$ AU. The hollow circles represent the orbits determined during the first opposition. The connected filled circles show the orbital elements computed including second opposition observations. 2 CKBOs were reclassified as Scattered KBOs, and 1 Scattered KBO was reclassified as a CKBO. In addition, 3 Resonant KBOs were reclassified as non-resonant objects.

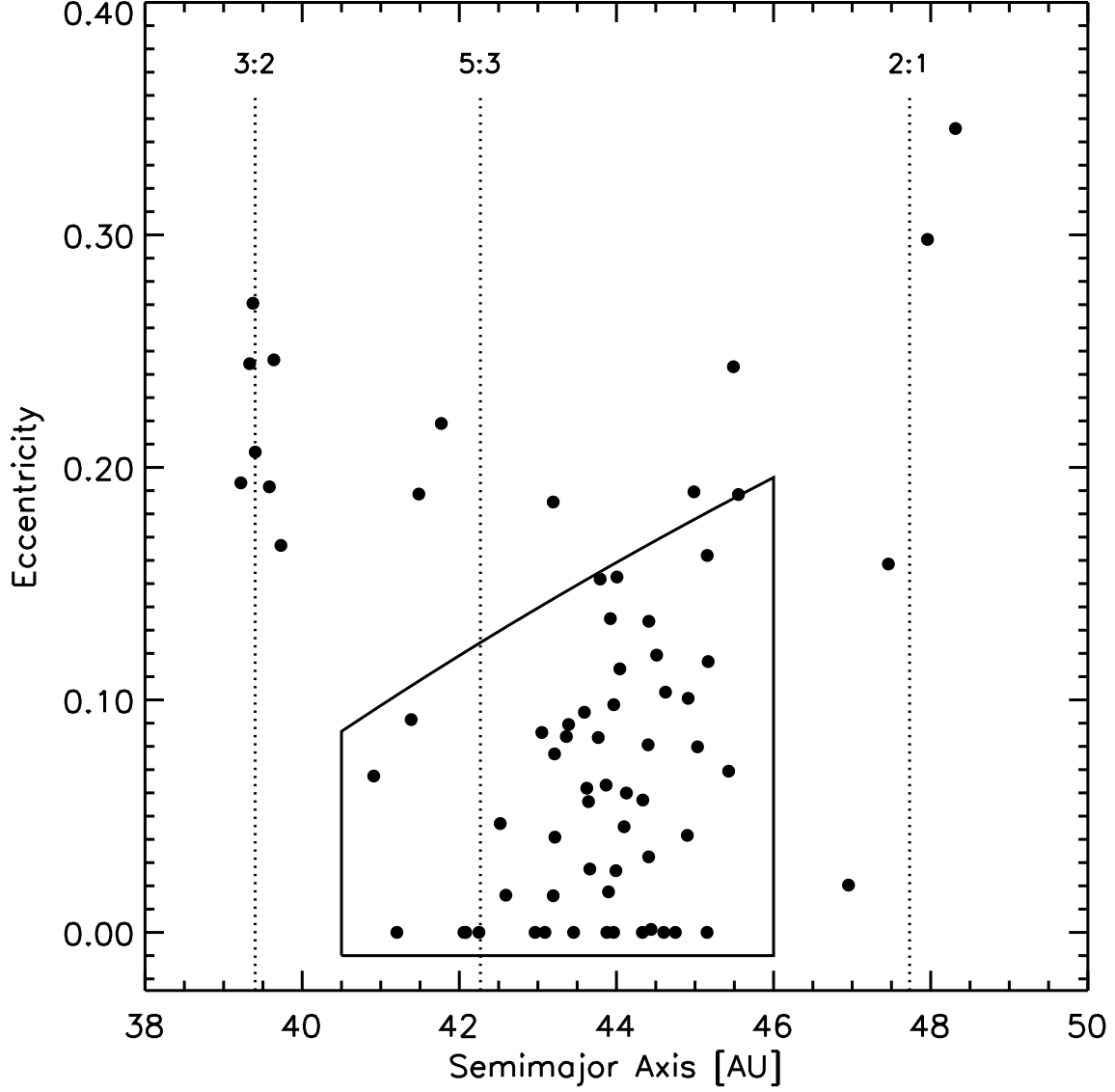


Fig. 6.— Eccentricity vs. semimajor axis of all KBOs discovered in this work with semimajor axes $a < 50$ AU. Note that few objects were found in the 3:2 resonance compared to previous studies. The area enclosed by a solid line indicates our criteria for selecting Classical KBOs, semimajor axes $40.5 \text{ AU} < a < 46 \text{ AU}$ and perihelia $q' > 37 \text{ AU}$.

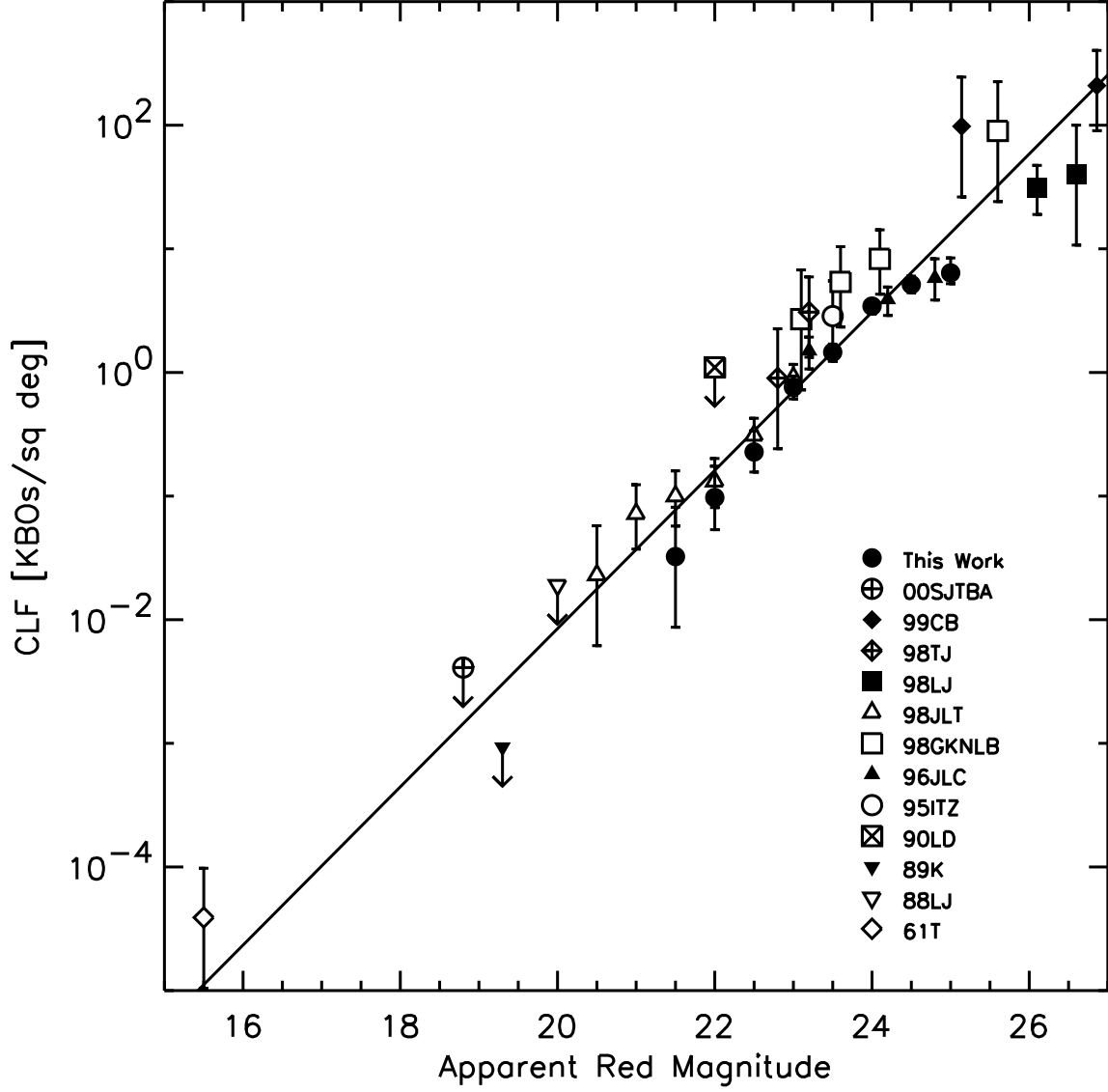


Fig. 7.— Our measurement of the Cumulative Luminosity Function (CLF), which represents the number of KBOs deg^{-2} near the ecliptic (filled circles) brighter than a given apparent red magnitude. Other points are previous works (see text for abbreviations), with arrows denoting upper limits. The line represents a fit to our data alone, yielding $\alpha = 0.63 \pm 0.06$, corresponding to $q = 4.15 \pm 0.3$ assuming the the albedo and heliocentric distance distributions are independent of the size distribution. Abbreviations are as follows: 00SJTBA is Sheppard et al. (2000), 99CB is Chiang & Brown (1999), 98GKNLB is Gladman et al. (1998), 98JLT is Jewitt, Luu & Trujillo (1998), 98LJ is Luu & Jewitt (1998), 98TJ is Trujillo & Jewitt (1998), 96JLC is Jewitt, Luu & Chen (1996), 95ITZ is Irwin, Tremaine & Żytkow (1995), 90LD is Levison & Duncan (1990), 89K is Kowal (1989), 88LJ is Luu & Jewitt (1988), and 61T is Tombaugh (1961).

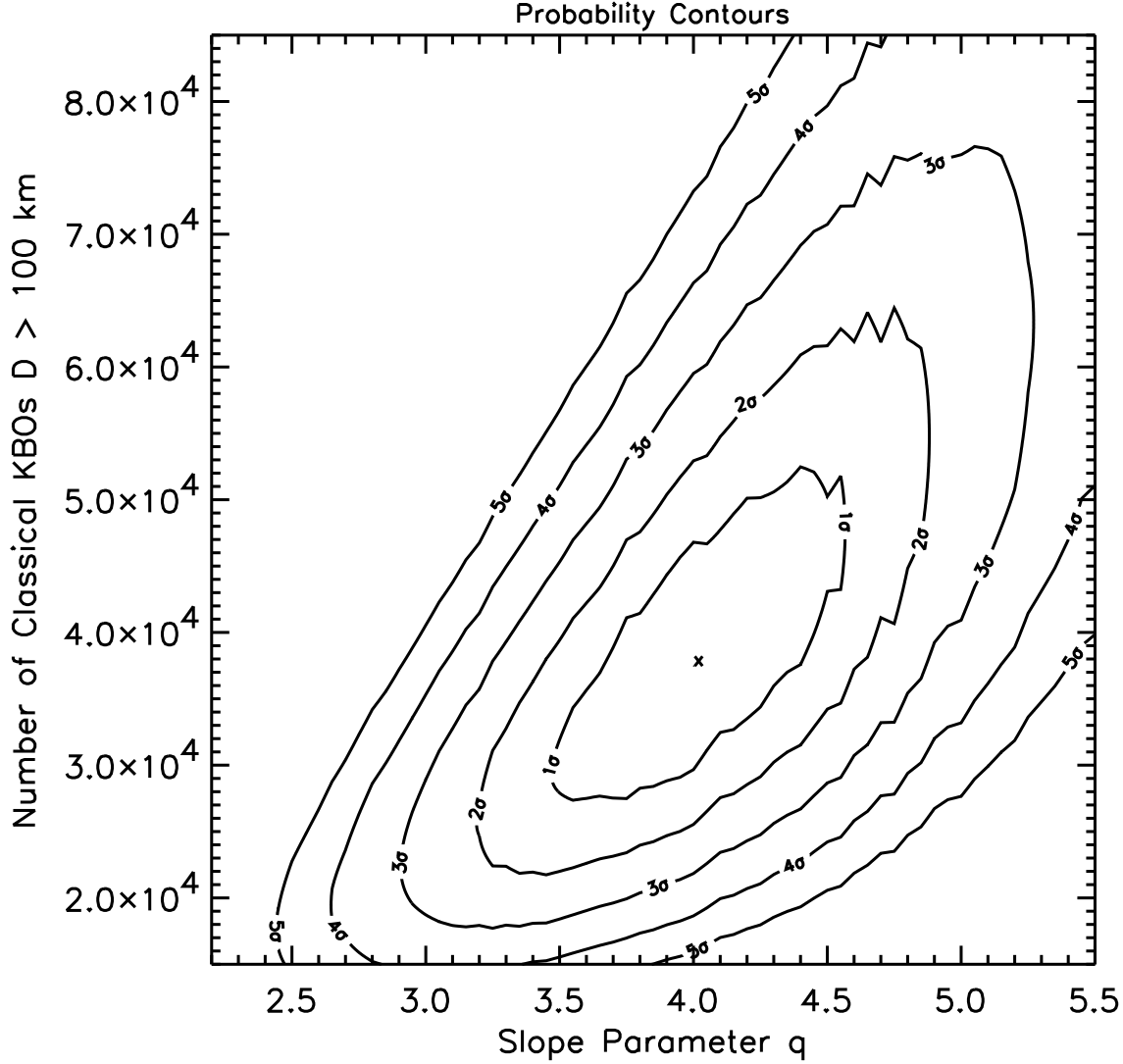


Fig. 8.— The maximum likelihood simulation of the size distribution power-law exponent. Contours of constant likelihood (1σ , 2σ , ... 5σ) are shown for a model with differential size distribution q (x-axis) and total number of objects greater than 100 km in diameter $N(D > 100 \text{ km})$ (y-axis). The maximum likelihood parameters (denoted by an x) occur at $q = 4.0$ and $N_{\text{CKBOs}}(D > 100 \text{ km}) = 3.8 \times 10^4$.

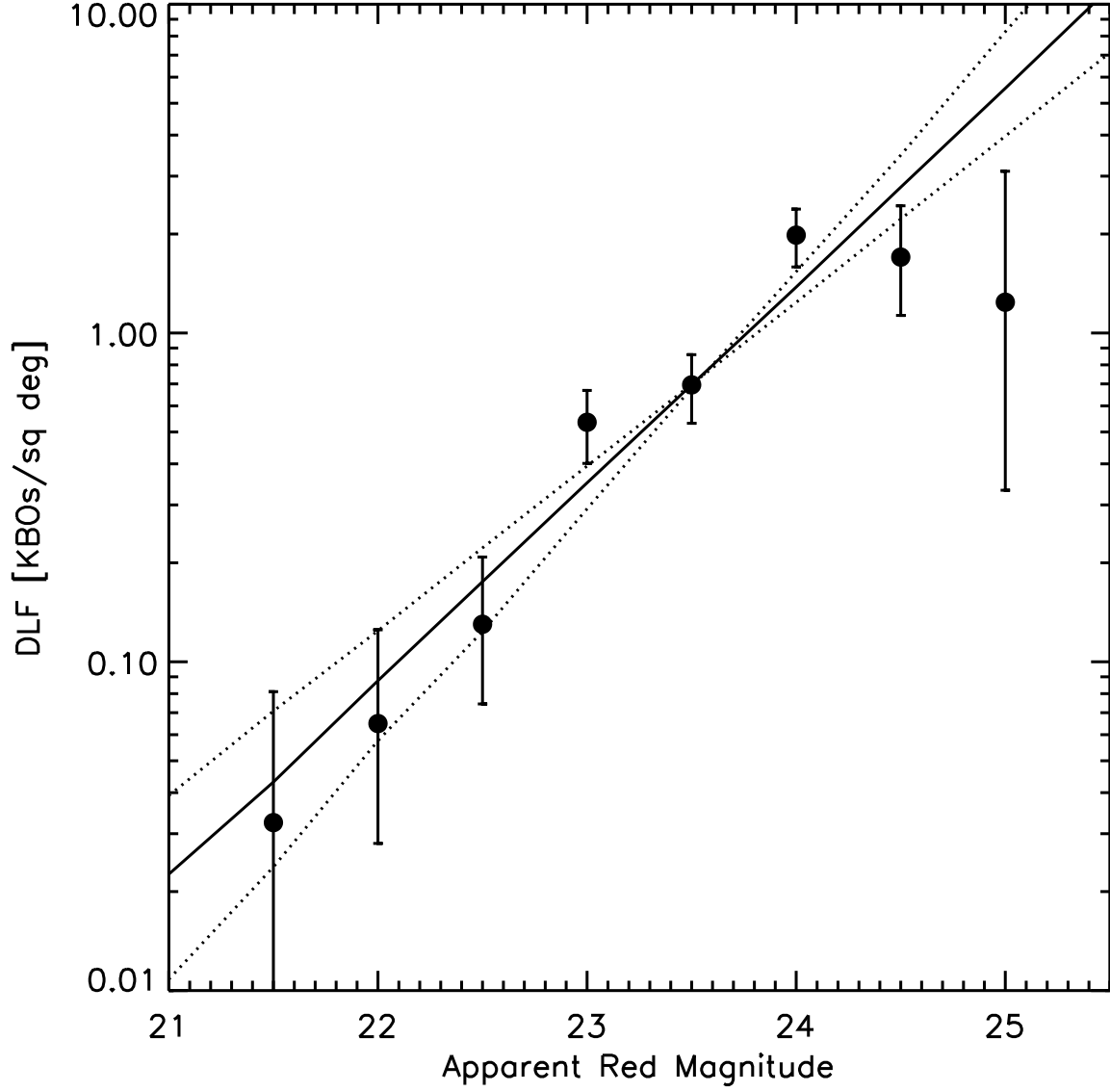


Fig. 9.— The Differential Luminosity Function (DLF), equal to the number of KBOs deg^{-2} near the ecliptic (filled circles). Three different models of the observed magnitude distribution are plotted from our maximum likelihood model (lines), representing the expected DLF for the $+1\sigma$ (dotted), best-fit (solid), and -1σ (dotted) cases of $q = 3.5$, 4.0, and 4.6, respectively.

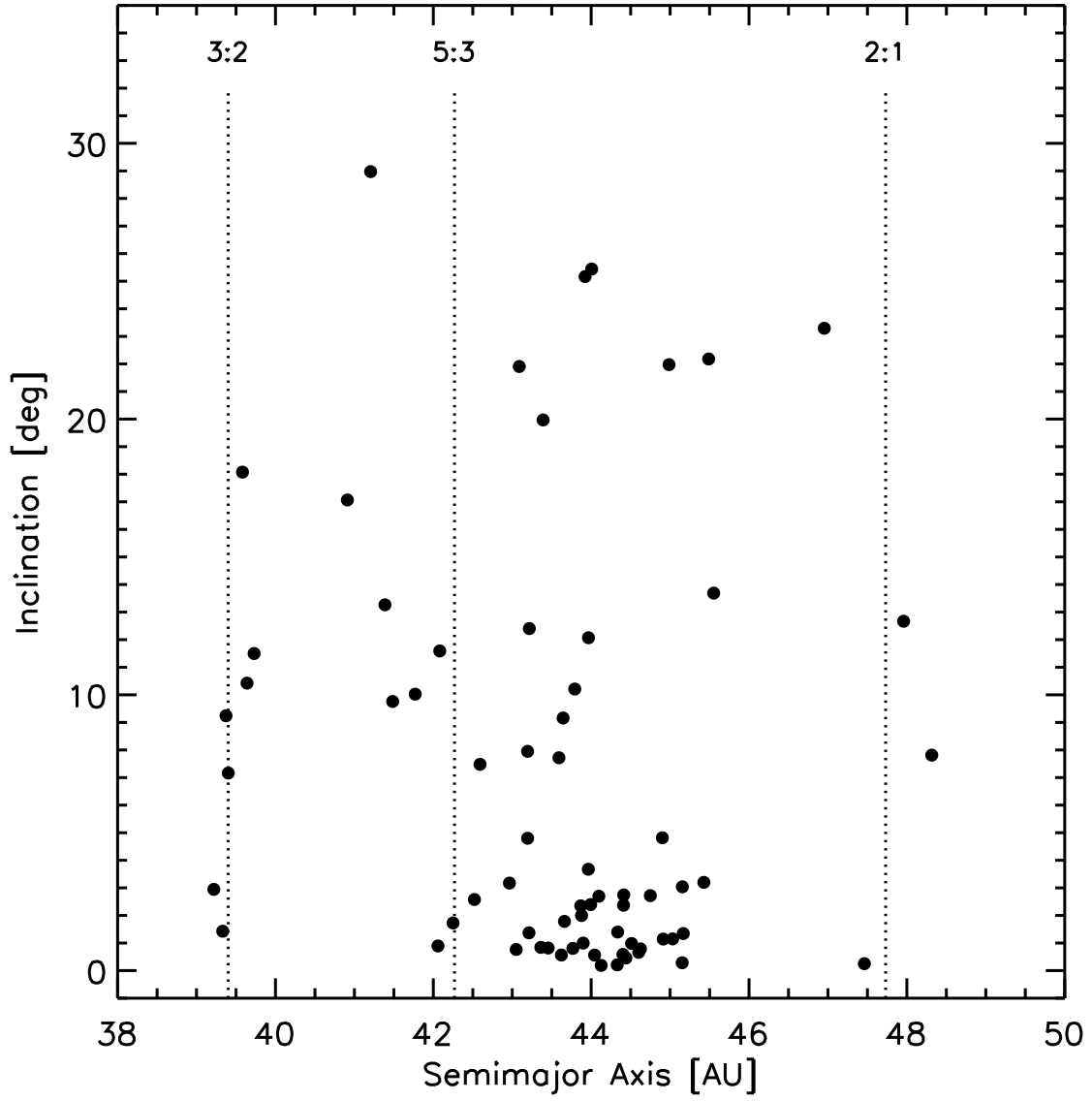


Fig. 10.— Inclination vs. semimajor axis of all KBOs discovered in this work with semimajor axes $a < 50$ AU.

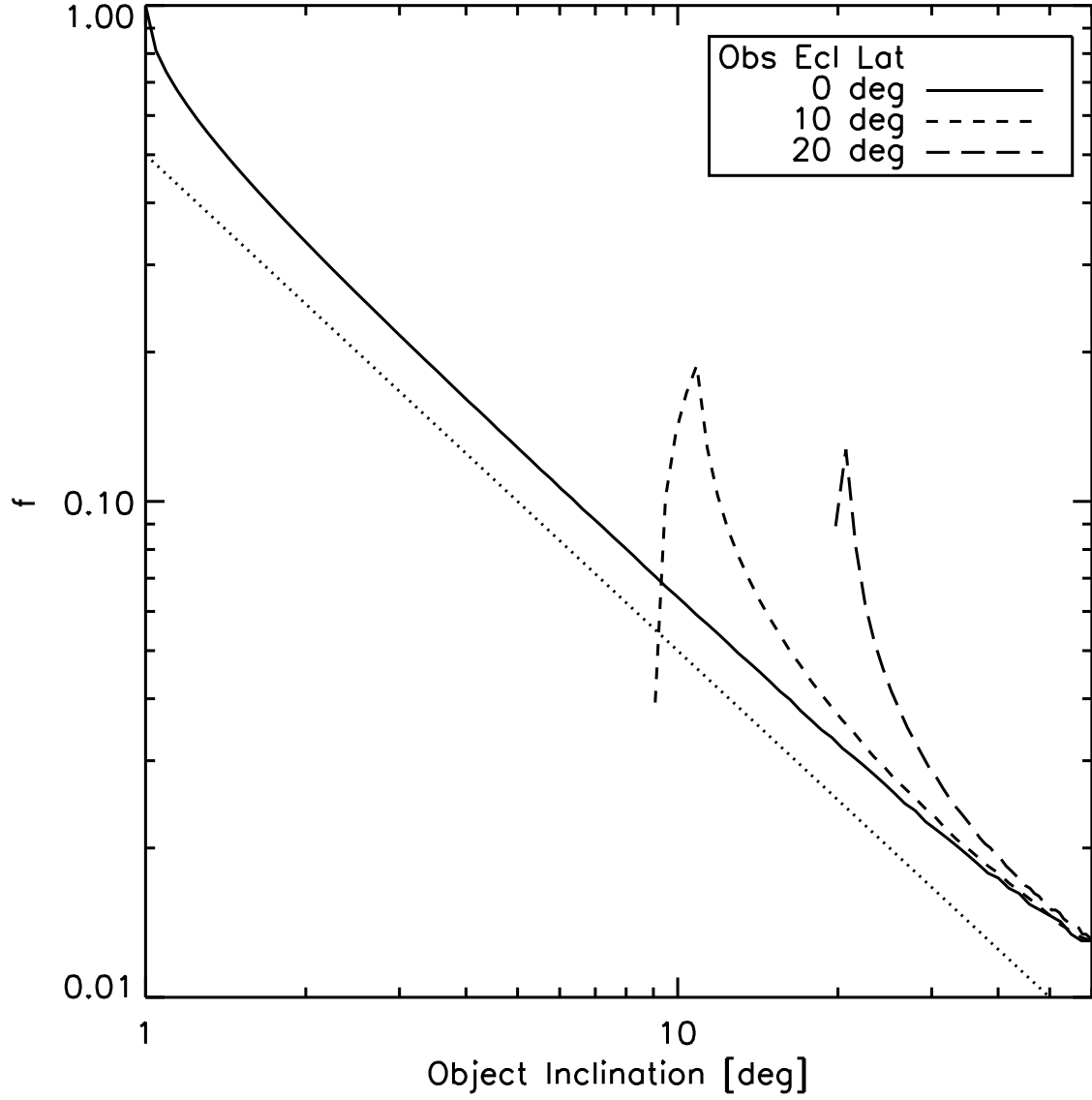


Fig. 11.— The fraction f of an orbit spent within $\pm 1^\circ$ (solid line), $10^\circ \pm 1^\circ$ (short dashed line), and $20^\circ \pm 1^\circ$ (long dashed line) of the ecliptic, as a function of object inclination i . The dotted line has a slope of $1/i$.

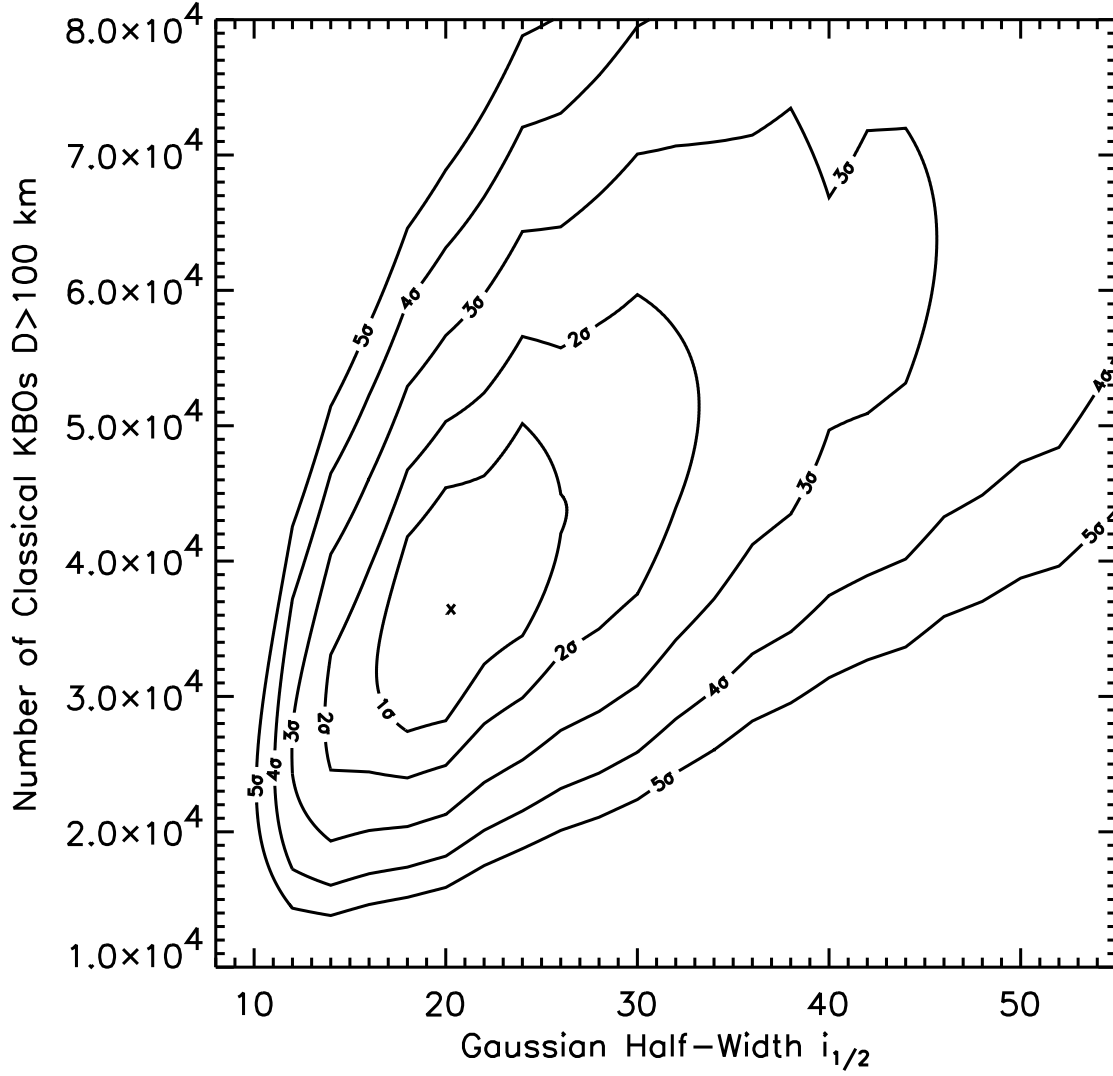


Fig. 12.— The maximum likelihood simulation. Contours of constant likelihood (1σ , 2σ , ... 5σ) are shown for a model with Gaussian half-width $i_{1/2}$ (x-axis) and total number of CKBOs with diameters greater than 100 km $N_{\text{CKBOs}}(D > 100 \text{ km})$ (y-axis). The maximum likelihood occurs at $N_{\text{CKBOs}}(D > 100 \text{ km}) = 3.8 \times 10^4$ and $i_{1/2} = 20^\circ$.

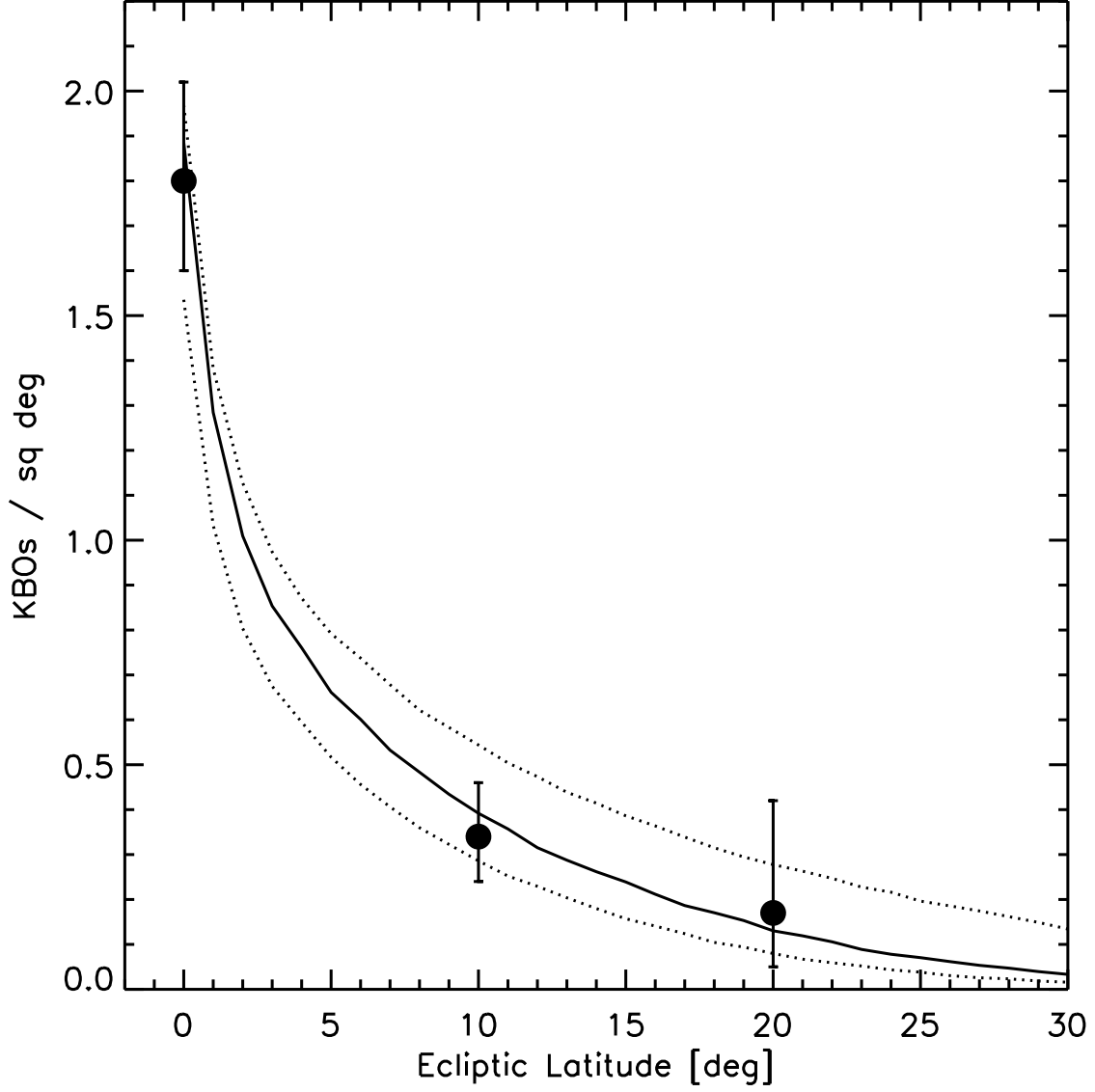


Fig. 13.— Surface density of KBOs brighter than $m_R = 23.7$ vs. ecliptic latitude. The solid line represents the best fit $i_{1/2} = 20^{+6}_{-4}^\circ$ CKBO model while the dotted lines represent the 1σ errors. The CKBO model has been multiplied by the observed KBO/CKBO ratio ($86/49 = 1.76$) for display purposes, to simulate the surface density of the more numerous KBOs.

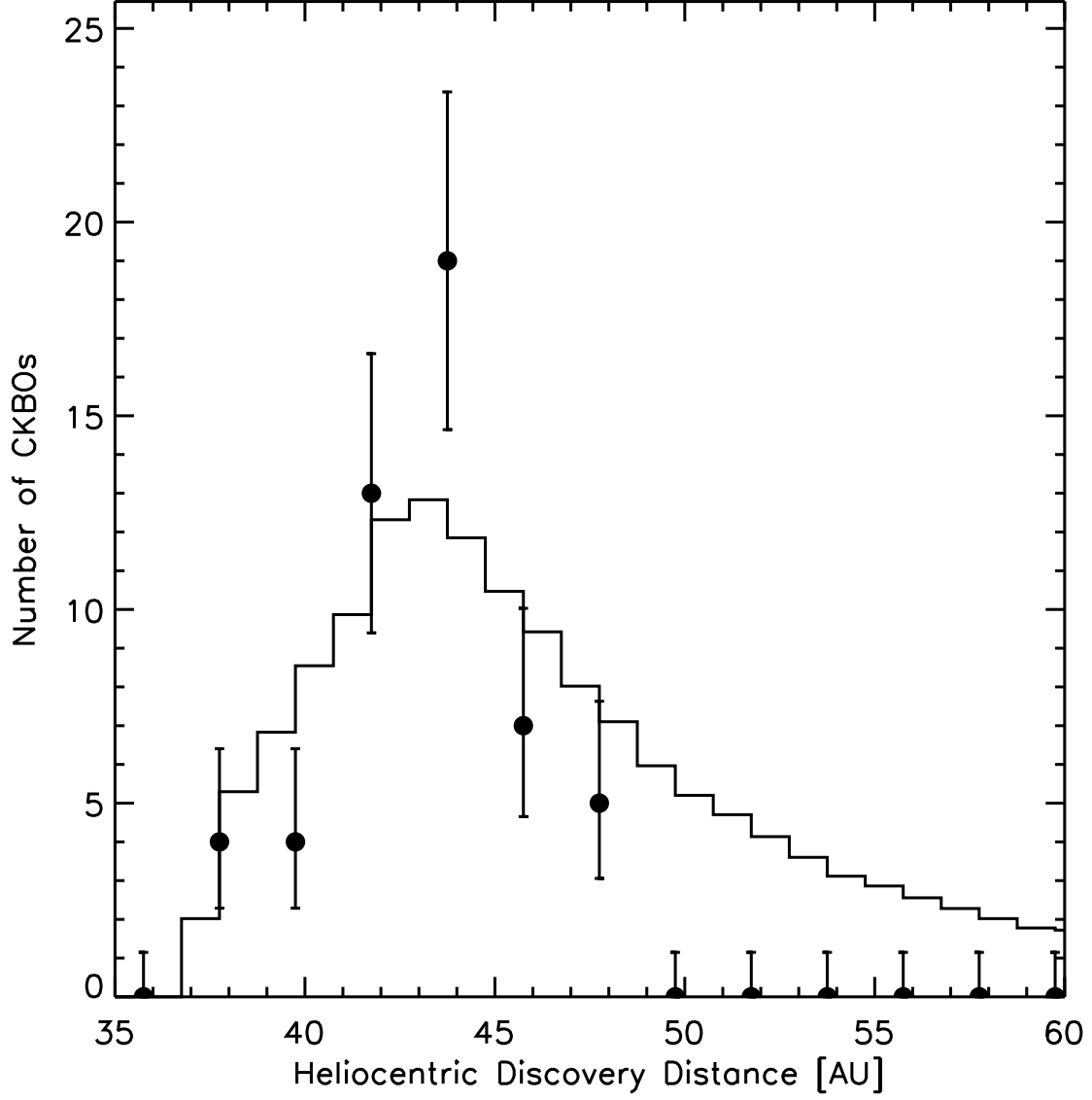


Fig. 14.— Observed heliocentric discovery distance (data points) and expected discoveries assuming the best-fit untruncated CKBO model (solid line). Note the very sharp drop in discovery statistics beginning at ~ 46 AU, violating the model. This is consistent with an outer edge to the Classical Kuiper Belt at 50 AU (3σ).

Table 1. CFHT Survey Parameters

| Quantity | CFHT 3.6m |
|---------------------------------|----------------------|
| Focal Ratio | f/4 |
| Instrument | CFHT 12k x 8k Mosaic |
| Plate Scale [arc sec/pixel] | 0.206 |
| North-South extent [deg] | 0.47 |
| East-West extent [deg] | 0.70 |
| Field Area [deg ²] | 0.330 |
| Total Area [deg ²] | 73 |
| Integration Time [sec] | 180 |
| Readout Time [sec] | 60 |
| m_{R50} ^a | 23.7 |
| θ ^b [arc sec] | 0.7–1.1 |
| Filter | <i>R</i> |
| Quantum Efficiency | 0.75 |

^athe red magnitude at which detection efficiency reaches half of the maximum efficiency

^bthe typical Full Width at Half Maximum of stellar sources for the surveys.

Table 2. CFHT 12k Photometric Calibration

| chip | $m_0 \pm \sigma$ | N |
|-----------------------|------------------|-----|
| Feb 1999 | | |
| 00 | 25.63 ± 0.03 | 2 |
| 01 | 25.74 ± 0.08 | 4 |
| 02 | 25.78 ± 0.08 | 7 |
| 03 | 26.07 ± 0.10 | 8 |
| 04 | 26.08 ± 0.08 | 6 |
| 05 | 26.06 ± 0.09 | 4 |
| 06 | not used | |
| 07 | 25.79 ± 0.04 | 4 |
| 08 | 26.00 ± 0.10 | 17 |
| 09 | 25.98 ± 0.05 | 6 |
| 10 | 26.03 ± 0.01 | 2 |
| 11 | 26.13 ± 0.04 | 2 |
| Sep 1999 and Mar 2000 | | |
| 00 (04 in Feb 1999) | 26.08 ± 0.05 | 6 |
| 01 | 25.74 ± 0.04 | 4 |
| 02 | 25.78 ± 0.05 | 7 |
| 03 ^a | 25.99 ± 0.09 | 3 |
| 04 (05 in Feb 1999) | 26.06 ± 0.08 | 4 |
| 05 (11 in Feb 1999) | 26.13 ± 0.04 | 2 |
| 06 ^a | 25.56 ± 0.02 | 5 |
| 07 | 25.79 ± 0.03 | 4 |
| 08 | 26.00 ± 0.10 | 17 |
| 09 | 25.98 ± 0.04 | 6 |
| 10 ^a | 25.49 ± 0.06 | 2 |
| 11 (03 in Feb 1999) | 26.07 ± 0.08 | 8 |

Note. — Zero points were consistent between observing runs, however, 3 chips were replaced and several of the remaining chips were shifted in position and renumbered after the Feb 1999 run.

^aNew chip added after Feb 1999 run.

Table 3. CFHT Field Centers

| ID | UT date | UT times | β ^a | α ^b | δ ^c | θ ^d | Objects | Chip |
|---------|-------------|-------------------|----------------------|-----------------------|-----------------------|-----------------------|------------------------|------|
| 476717o | 1999 Feb 10 | 06:43 07:59 09:04 | 0.0 | 08:02:20 | 20:28:05 | m | 1999 CD ₁₅₈ | 10 |
| 476718o | 1999 Feb 10 | 06:49 08:04 09:09 | 0.0 | 08:06:35 | 20:15:31 | m | | |
| 476719o | 1999 Feb 10 | 06:55 08:09 09:14 | 0.0 | 08:10:49 | 20:02:35 | m | | |
| 476720o | 1999 Feb 10 | 07:00 08:13 09:19 | 0.0 | 08:15:03 | 19:49:15 | m | | |
| 476721o | 1999 Feb 10 | 07:05 08:19 09:24 | 0.0 | 08:19:16 | 19:35:34 | m | 1999 CV ₁₁₈ | 05 |
| 476722o | 1999 Feb 10 | 07:10 08:24 09:28 | 0.0 | 08:23:27 | 19:21:32 | p | | |
| 476723o | 1999 Feb 10 | 07:15 08:29 09:33 | 0.0 | 08:27:39 | 19:06:36 | p | | |
| 476724o | 1999 Feb 10 | 07:19 08:33 09:38 | 0.0 | 08:31:49 | 18:51:58 | p | | |
| 476725o | 1999 Feb 10 | 07:24 08:39 09:43 | 0.0 | 08:35:59 | 18:36:59 | p | 1999 CP ₁₅₃ | 05 |
| 476726o | 1999 Feb 10 | 07:29 08:43 09:48 | 0.0 | 08:40:07 | 18:21:52 | p | 1999 CK ₁₅₈ | 00 |
| 476727o | 1999 Feb 10 | 07:34 08:49 09:53 | 0.0 | 08:44:15 | 18:06:06 | g | | |
| 476728o | 1999 Feb 10 | 07:39 08:54 09:57 | 0.0 | 08:48:23 | 17:49:36 | g | | |
| 476729o | 1999 Feb 10 | 07:44 08:59 10:02 | 0.0 | 08:52:29 | 17:33:16 | g | | |
| 476758o | 1999 Feb 10 | 10:17 11:16 12:23 | 0.0 | 11:00:58 | 06:18:15 | g | 1999 CY ₁₁₈ | 03 |
| 476759o | 1999 Feb 10 | 10:22 11:21 12:28 | 0.0 | 11:04:41 | 05:54:46 | g | 1999 CZ ₁₁₈ | 05 |
| 476760o | 1999 Feb 10 | 10:27 11:27 12:33 | 0.0 | 11:08:24 | 05:31:46 | g | | |
| 476761o | 1999 Feb 10 | 10:32 11:31 12:38 | 0.0 | 11:12:06 | 05:08:30 | g | | |
| | | | | | | | | |
| | | | | | | | 1999 CA ₁₁₉ | 03 |
| | | | | | | | 1999 CW ₁₁₈ | 04 |
| | | | | | | | 1999 CB ₁₁₉ | 07 |
| 476762o | 1999 Feb 10 | 10:37 11:36 12:43 | 0.0 | 11:15:47 | 04:45:05 | g | 1999 CC ₁₁₉ | 07 |
| 476763o | 1999 Feb 10 | 10:42 11:41 12:48 | 0.0 | 11:19:29 | 04:21:28 | g | | |
| 476764o | 1999 Feb 10 | 10:47 11:46 12:53 | 0.0 | 11:23:11 | 03:57:53 | g | | |
| 476765o | 1999 Feb 10 | 10:52 11:51 12:57 | 0.0 | 11:26:51 | 03:34:20 | g | | |
| 476766o | 1999 Feb 10 | 10:57 11:56 13:03 | 0.0 | 11:30:32 | 03:10:51 | g | 1999 CD ₁₁₉ | 02 |
| 476767o | 1999 Feb 10 | 11:02 12:01 13:08 | 0.0 | 11:34:12 | 02:47:19 | g | | |
| 476768o | 1999 Feb 10 | 11:07 12:06 13:13 | 0.0 | 11:37:52 | 02:23:46 | g | | |
| 476769o | 1999 Feb 10 | 11:12 12:11 13:18 | 0.0 | 11:41:32 | 01:59:58 | g | | |
| 476795o | 1999 Feb 10 | 13:22 14:12 15:25 | 0.5 | 11:00:58 | 06:48:07 | g | C79710 | 10 |
| 476796o | 1999 Feb 10 | 13:28 14:17 15:30 | 0.5 | 11:04:41 | 06:25:10 | g | | |
| 476797o | 1999 Feb 10 | 13:33 14:21 15:35 | 0.5 | 11:08:23 | 06:01:54 | g | | |
| 476798o | 1999 Feb 10 | 13:38 14:26 15:40 | 0.5 | 11:12:06 | 05:38:39 | m | | |
| 476799o | 1999 Feb 10 | 13:43 14:31 15:45 | 0.5 | 11:15:48 | 05:14:56 | m | C79900 | 00 |
| 476848o | 1999 Feb 11 | 06:25 07:24 08:22 | 0.5 | 08:02:20 | 20:57:35 | g | | |
| 476849o | 1999 Feb 11 | 06:30 07:29 08:27 | 0.5 | 08:06:35 | 20:45:02 | g | | |
| 476850o | 1999 Feb 11 | 06:35 07:34 08:31 | 0.5 | 08:10:49 | 20:32:00 | g | | |
| 476851o | 1999 Feb 11 | 06:39 07:40 08:36 | 0.5 | 08:15:03 | 20:18:49 | g | 1999 CF ₁₁₉ | 10 |

Table 3—Continued

| ID | UT date | UT times | β ^a | α ^b | δ ^c | θ ^d | Objects | Chip |
|---------|-------------|-------------------|----------------------|-----------------------|-----------------------|-----------------------|------------------------|------|
| 476852o | 1999 Feb 11 | 06:44 07:45 08:41 | 0.5 | 08:19:15 | 20:05:13 | g | 1999 CG ₁₁₉ | 00 |
| | | | | | | | 1999 CL ₁₅₈ | 04 |
| 476853o | 1999 Feb 11 | 06:49 07:49 08:45 | 0.5 | 08:23:28 | 19:51:00 | g | 1999 CH ₁₁₉ | 00 |
| 476854o | 1999 Feb 11 | 06:53 07:54 08:52 | 0.5 | 08:27:39 | 19:36:42 | g | 1999 CS ₁₅₃ | 04 |
| | | | | | | | C85410 | 10 |
| 476855o | 1999 Feb 11 | 06:58 07:58 08:56 | 0.5 | 08:31:49 | 19:21:54 | g | 1999 CK ₁₁₉ | 04 |
| | | | | | | | 1999 CJ ₁₁₉ | 09 |
| 476856o | 1999 Feb 11 | 07:03 08:03 09:01 | 0.5 | 08:35:59 | 19:06:54 | g | 1999 CL ₁₁₉ | 00 |
| 476857o | 1999 Feb 11 | 07:08 08:08 09:06 | 0.5 | 08:40:08 | 18:51:15 | g | 1999 CM ₁₁₉ | 00 |
| 476858o | 1999 Feb 11 | 07:12 08:12 09:10 | 0.5 | 08:44:16 | 18:35:49 | g | 1999 CG ₁₅₄ | 08 |
| 476859o | 1999 Feb 11 | 07:19 08:17 09:16 | 0.5 | 08:48:22 | 18:19:42 | g | 1999 CN ₁₁₉ | 04 |
| | | | | | | | 1999 CX ₁₃₁ | 07 |
| | | | | | | | C85909 | 09 |
| 476885o | 1999 Feb 11 | 09:30 10:25 11:22 | 0.0 | 10:00:16 | 12:12:18 | g | 1999 CM ₁₅₃ | 05 |
| 476886o | 1999 Feb 11 | 09:35 10:30 11:26 | 0.0 | 10:04:07 | 11:51:18 | g | 1999 CY ₁₃₁ | 00 |
| | | | | | | | C88608 | 08 |
| 476887o | 1999 Feb 11 | 09:39 10:35 11:31 | 0.0 | 10:07:59 | 11:30:17 | g | | |
| 476888o | 1999 Feb 11 | 09:44 10:39 11:36 | 0.0 | 10:11:51 | 11:08:42 | g | | |
| 476889o | 1999 Feb 11 | 09:48 10:44 11:40 | 0.0 | 10:15:41 | 10:47:11 | g | 1999 CZ ₁₃₁ | 02 |
| | | | | | | | C88905 | 05 |
| 476890o | 1999 Feb 11 | 09:53 10:48 11:45 | 0.0 | 10:19:31 | 10:25:24 | g | 1999 CN ₁₅₃ | 00 |
| 476891o | 1999 Feb 11 | 09:58 10:53 11:50 | 0.0 | 10:23:19 | 10:03:45 | g | | |
| 476892o | 1999 Feb 11 | 10:02 10:58 11:55 | 0.0 | 10:27:08 | 09:41:46 | g | | |
| 476893o | 1999 Feb 11 | 10:07 11:03 11:59 | 0.0 | 10:30:56 | 09:19:30 | g | 1999 CA ₁₃₂ | 01 |
| 476894o | 1999 Feb 11 | 10:11 11:07 12:04 | 0.0 | 10:34:43 | 08:57:18 | g | | |
| 476895o | 1999 Feb 11 | 10:16 11:12 12:09 | 0.0 | 10:38:30 | 08:35:00 | g | 1999 CQ ₁₅₃ | 00 |
| | | | | | | | 1999 DC ₂ | 03 |
| | | | | | | | 1999 CP ₁₃₃ | 07 |
| 476896o | 1999 Feb 11 | 10:21 11:17 12:14 | 0.0 | 10:42:16 | 08:12:28 | g | | |
| 476924o | 1999 Feb 11 | 12:36 13:35 14:37 | -0.5 | 10:53:31 | 06:34:12 | g | 1999 CM ₁₅₈ | 11 |
| 476984o | 1999 Feb 12 | 06:05 07:06 08:17 | -0.5 | 08:06:36 | 19:45:05 | g | | |
| 476985o | 1999 Feb 12 | 06:10 07:11 08:22 | -0.5 | 08:10:50 | 19:31:54 | g | | |
| 476986o | 1999 Feb 12 | 06:14 07:15 08:26 | -0.5 | 08:15:03 | 19:18:44 | g | 1999 CQ ₁₃₃ | 02 |
| | | | | | | | 1999 CO ₁₅₃ | 03 |
| 476987o | 1999 Feb 12 | 06:19 07:20 08:31 | -0.5 | 08:19:16 | 19:04:59 | g | 1999 CR ₁₃₃ | 03 |
| 476988o | 1999 Feb 12 | 06:24 07:25 08:36 | -0.5 | 08:23:28 | 18:51:00 | g | | |

Table 3—Continued

| ID | UT date | UT times | β ^a | α ^b | δ ^c | θ ^d | Objects | Chip |
|---------|-------------|-------------------|----------------------|-----------------------|-----------------------|-----------------------|------------------------|------|
| 476989o | 1999 Feb 12 | 06:28 07:32 08:41 | -0.5 | 08:27:39 | 18:36:36 | g | | |
| 476990o | 1999 Feb 12 | 06:33 07:37 08:45 | -0.5 | 08:31:49 | 18:21:49 | g | | |
| 476991o | 1999 Feb 12 | 06:38 07:41 08:50 | -0.5 | 08:35:59 | 18:06:50 | g | | |
| 476992o | 1999 Feb 12 | 06:42 07:46 08:55 | -0.5 | 08:40:08 | 17:51:13 | m | | |
| 476993o | 1999 Feb 12 | 06:47 07:51 09:00 | -0.5 | 08:44:16 | 17:35:35 | m | | |
| 476994o | 1999 Feb 12 | 06:52 07:55 09:04 | -0.5 | 08:48:23 | 17:19:42 | m | 1999 CU ₁₅₃ | 11 |
| 476995o | 1999 Feb 12 | 06:56 08:00 09:09 | -0.5 | 08:52:29 | 17:03:11 | m | 1999 CH ₁₅₄ | 02 |
| 476996o | 1999 Feb 12 | 07:01 08:05 09:14 | -0.5 | 08:56:35 | 16:46:16 | m | | |
| 477025o | 1999 Feb 12 | 09:27 10:23 12:36 | -10 | 10:00:15 | 02:12:25 | p | | |
| 477026o | 1999 Feb 12 | 09:31 10:27 12:41 | -10 | 10:04:07 | 01:51:27 | p | | |
| 477027o | 1999 Feb 12 | 09:36 10:32 12:46 | -10 | 10:07:59 | 01:30:14 | m | | |
| 477028o | 1999 Feb 12 | 09:40 10:37 12:51 | -10 | 10:11:50 | 01:08:57 | g | | |
| 477029o | 1999 Feb 12 | 09:45 10:42 12:56 | -10 | 10:15:40 | 00:47:11 | g | | |
| 477030o | 1999 Feb 12 | 09:50 10:46 13:00 | -10 | 10:19:31 | 00:25:29 | g | | |
| 477031o | 1999 Feb 12 | 09:55 10:51 13:05 | -10 | 10:23:19 | 00:03:42 | g | | |
| 477032o | 1999 Feb 12 | 09:59 10:56 13:18 | -10 | 10:27:07 | -00:18:10 | g | | |
| 477033o | 1999 Feb 12 | 10:04 11:00 13:23 | -10 | 10:30:55 | -00:40:21 | g | | |
| 477034o | 1999 Feb 12 | 10:09 11:05 13:27 | -10 | 10:34:43 | -01:02:47 | g | | |
| 477035o | 1999 Feb 12 | 10:13 11:10 13:32 | -10 | 10:38:29 | -01:25:03 | g | | |
| 477036o | 1999 Feb 12 | 10:18 11:14 13:36 | -10 | 10:42:16 | -01:47:48 | g | | |
| 477159o | 1999 Feb 15 | 06:53 08:12 09:09 | 10 | 08:10:49 | 30:02:21 | p | | |
| 477161o | 1999 Feb 15 | 07:06 08:17 09:14 | 10 | 08:15:02 | 29:48:41 | p | | |
| 477162o | 1999 Feb 15 | 07:11 08:21 09:19 | 10 | 08:19:15 | 29:35:18 | m | | |
| 477163o | 1999 Feb 15 | 07:17 08:26 09:23 | 10 | 08:23:27 | 29:20:55 | p | | |
| 477164o | 1999 Feb 15 | 07:24 08:31 09:28 | 10 | 08:27:38 | 29:06:46 | p | | |
| 477165o | 1999 Feb 15 | 07:29 08:36 09:33 | 10 | 08:31:49 | 28:51:51 | g | | |
| 477166o | 1999 Feb 15 | 07:33 08:41 09:37 | 10 | 08:35:59 | 28:36:50 | m | | |
| 477167o | 1999 Feb 15 | 07:38 08:46 09:42 | 10 | 08:40:07 | 28:21:24 | m | | |
| 477168o | 1999 Feb 15 | 07:43 08:50 09:46 | 10 | 08:44:16 | 28:06:06 | m | | |
| 477169o | 1999 Feb 15 | 07:50 08:55 09:54 | 10 | 08:48:23 | 27:49:29 | p | | |
| 477170o | 1999 Feb 15 | 07:56 09:00 09:59 | 10 | 08:52:29 | 27:33:09 | p | 1999 CC ₁₅₈ | 00 |
| 477171o | 1999 Feb 15 | 08:01 09:04 10:03 | 10 | 08:56:34 | 27:16:38 | p | | |
| 477198o | 1999 Feb 15 | 10:17 11:10 12:01 | -10 | 09:16:50 | 05:48:46 | m | | |
| 477199o | 1999 Feb 15 | 10:22 11:15 12:06 | -10 | 09:20:50 | 05:30:28 | g | | |
| 477200o | 1999 Feb 15 | 10:27 11:20 12:11 | -10 | 09:24:50 | 05:11:47 | g | | |
| 477201o | 1999 Feb 15 | 10:32 11:24 12:16 | -10 | 09:28:49 | 04:52:47 | g | | |

Table 3—Continued

| ID | UT date | UT times | β ^a | α ^b | δ ^c | θ ^d | Objects | Chip |
|---------|-------------|-------------------|----------------------|-----------------------|-----------------------|-----------------------|------------------------|------|
| 477202o | 1999 Feb 15 | 10:36 11:29 12:20 | -10 | 09:32:47 | 04:33:40 | g | | |
| 477203o | 1999 Feb 15 | 10:41 11:33 12:25 | -10 | 09:36:45 | 04:14:10 | m | | |
| 477204o | 1999 Feb 15 | 10:46 11:38 12:30 | -10 | 09:40:42 | 03:54:17 | m | | |
| 477205o | 1999 Feb 15 | 10:50 11:43 12:34 | -10 | 09:44:38 | 03:34:14 | p | | |
| 477206o | 1999 Feb 15 | 10:55 11:47 12:39 | -10 | 09:48:33 | 03:14:07 | g | | |
| 477207o | 1999 Feb 15 | 11:01 11:52 12:43 | -10 | 09:52:28 | 02:53:53 | g | | |
| 477208o | 1999 Feb 15 | 11:05 11:57 12:48 | -10 | 09:56:21 | 02:33:19 | g | | |
| 477232o | 1999 Feb 15 | 13:00 13:50 14:50 | 10 | 10:53:30 | 17:04:13 | p | | |
| 477233o | 1999 Feb 15 | 13:04 14:02 14:54 | 10 | 10:57:14 | 16:41:09 | p | | |
| 477234o | 1999 Feb 15 | 13:09 14:07 14:59 | 10 | 11:00:57 | 16:18:09 | p | | |
| 477235o | 1999 Feb 15 | 13:13 14:11 15:07 | 10 | 11:04:41 | 15:54:58 | m | | |
| 477236o | 1999 Feb 15 | 13:18 14:16 15:12 | 10 | 11:08:23 | 15:31:42 | m | | |
| 477237o | 1999 Feb 15 | 13:23 14:20 15:17 | 10 | 11:12:06 | 15:08:20 | p | | |
| 477238o | 1999 Feb 15 | 13:27 14:25 15:22 | 10 | 11:15:47 | 14:44:54 | m | | |
| 477239o | 1999 Feb 15 | 13:32 14:30 15:27 | 10 | 11:19:29 | 14:21:38 | m | | |
| 477240o | 1999 Feb 15 | 13:37 14:35 15:32 | 10 | 11:23:10 | 13:57:52 | m | | |
| 477241o | 1999 Feb 15 | 13:41 14:39 15:36 | 10 | 11:26:51 | 13:34:26 | m | | |
| 477242o | 1999 Feb 15 | 13:46 14:45 15:41 | 10 | 11:30:32 | 13:10:40 | m | | |
| 502047o | 1999 Sep 06 | 06:15 07:21 08:27 | 0.0 | 21:21:27 | -15:28:08 | g | 1999 RS ₂₁₄ | 00 |
| | | | | | | | 1999 RT ₂₁₄ | 07 |
| 502048o | 1999 Sep 06 | 06:20 07:26 08:33 | 0.0 | 21:25:14 | -15:10:14 | g | | |
| 502049o | 1999 Sep 06 | 06:25 07:30 08:37 | 0.0 | 21:29:01 | -14:52:18 | g | 1999 RU ₂₁₄ | 10 |
| 502050o | 1999 Sep 06 | 06:29 07:36 08:42 | 0.0 | 21:32:47 | -14:34:08 | m | | |
| 502051o | 1999 Sep 06 | 06:34 07:40 08:47 | 0.0 | 21:36:32 | -14:15:08 | m | 1999 RV ₂₁₄ | 05 |
| 502052o | 1999 Sep 06 | 06:39 07:45 08:52 | 0.0 | 21:40:17 | -13:56:27 | m | | |
| 502053o | 1999 Sep 06 | 06:44 07:50 08:57 | 10 | 21:21:27 | -05:28:08 | m | | |
| 502054o | 1999 Sep 06 | 06:49 07:55 09:01 | 10 | 21:25:14 | -05:09:51 | m | | |
| 502055o | 1999 Sep 06 | 06:53 08:00 09:06 | 10 | 21:29:00 | -04:51:51 | m | | |
| 502056o | 1999 Sep 06 | 06:58 08:04 09:11 | 10 | 21:32:47 | -04:34:07 | m | | |
| 502057o | 1999 Sep 06 | 07:03 08:09 09:16 | 10 | 21:36:32 | -04:15:09 | m | | |
| 502058o | 1999 Sep 06 | 07:08 08:14 09:21 | 10 | 21:40:17 | -03:56:27 | g | | |
| 502098o | 1999 Sep 06 | 09:38 10:58 11:49 | 0.0 | 00:05:31 | 00:35:33 | m | 1999 RW ₂₁₄ | 04 |
| 502099o | 1999 Sep 06 | 09:43 11:00 11:54 | 0.0 | 00:09:07 | 00:58:31 | m | | |
| 502100o | 1999 Sep 06 | 09:48 11:05 11:59 | 0.0 | 00:12:43 | 01:21:56 | m | | |
| 502101o | 1999 Sep 06 | 09:53 10:49 12:03 | 0.0 | 00:16:18 | 01:45:51 | m | | |
| 502102o | 1999 Sep 06 | 09:58 11:10 12:09 | 0.0 | 00:19:55 | 02:08:38 | g | | |

Table 3—Continued

| ID | UT date | UT times | β ^a | α ^b | δ ^c | θ ^d | Objects | Chip |
|---------|-------------|-------------------|----------------------|-----------------------|-----------------------|-----------------------|------------------------|------|
| 502103o | 1999 Sep 06 | 10:03 11:14 12:13 | 0.0 | 00:23:31 | 02:32:01 | m | 1999 RX ₂₁₄ | 00 |
| 502104o | 1999 Sep 06 | 10:08 11:19 12:18 | 10 | 00:05:31 | 10:35:05 | m | | |
| 502105o | 1999 Sep 06 | 10:14 11:25 12:23 | 10 | 00:09:06 | 10:59:08 | m | | |
| 502106o | 1999 Sep 06 | 10:20 11:30 12:28 | 10 | 00:12:43 | 11:21:53 | m | | |
| 502107o | 1999 Sep 06 | 10:26 11:34 12:32 | 10 | 00:16:18 | 11:45:38 | m | | |
| 502108o | 1999 Sep 06 | 10:31 11:39 12:37 | 10 | 00:19:55 | 12:08:38 | m | 1999 RY ₂₁₄ | 01 |
| 502109o | 1999 Sep 06 | 10:36 11:44 12:42 | 10 | 00:23:31 | 12:32:32 | m | 1999 RZ ₂₁₄ | 08 |
| 502136o | 1999 Sep 06 | 12:57 13:41 14:33 | 0.0 | 00:27:08 | 02:55:33 | m | 1999 RB ₂₁₅ | 01 |
| | | | | | | | 1999 RC ₂₁₅ | 04 |
| 502137o | 1999 Sep 06 | 13:02 13:45 14:38 | 0.0 | 00:30:45 | 03:19:07 | m | 1999 RD ₂₁₅ | 09 |
| 502138o | 1999 Sep 06 | 13:06 14:00 14:47 | 0.0 | 00:34:22 | 03:42:21 | m | | |
| 502139o | 1999 Sep 06 | 13:11 14:05 14:56 | 0.0 | 00:38:00 | 04:05:33 | g | | |
| 502140o | 1999 Sep 06 | 13:16 14:09 14:51 | 0.0 | 00:41:38 | 04:28:42 | m | | |
| 502141o | 1999 Sep 06 | 13:21 14:14 15:01 | 10 | 00:27:08 | 12:55:51 | g | | |
| 502142o | 1999 Sep 06 | 13:25 14:19 15:06 | 10 | 00:30:46 | 13:18:40 | g | | |
| 502143o | 1999 Sep 06 | 13:30 14:24 15:11 | 10 | 00:34:23 | 13:41:59 | m | | |
| 502182o | 1999 Sep 07 | 07:03 07:53 08:40 | 0.0 | 21:44:02 | -13:37:58 | m | 1999 RE ₂₁₅ | 04 |
| 502183o | 1999 Sep 07 | 07:08 07:57 08:46 | 0.0 | 21:47:45 | -13:18:51 | g | | |
| 502184o | 1999 Sep 07 | 07:14 08:02 08:51 | 0.0 | 21:51:28 | -12:59:04 | g | | |
| 502185o | 1999 Sep 07 | 07:19 08:07 08:57 | 0.0 | 21:55:11 | -12:39:55 | m | | |
| 502186o | 1999 Sep 07 | 07:24 08:12 09:02 | 0.0 | 21:58:54 | -12:20:10 | m | 1999 RF ₂₁₅ | 06 |
| 502187o | 1999 Sep 07 | 07:29 08:17 09:06 | 10 | 21:44:01 | -03:38:03 | m | 1999 RG ₂₁₅ | 02 |
| 502188o | 1999 Sep 07 | 07:33 08:21 09:11 | 10 | 21:47:45 | -03:18:57 | g | | |
| 502189o | 1999 Sep 07 | 07:38 08:26 09:16 | 10 | 21:51:28 | -02:59:34 | m | | |
| 502190o | 1999 Sep 07 | 07:43 08:31 09:21 | 10 | 21:55:11 | -02:39:32 | m | | |
| 502191o | 1999 Sep 07 | 07:47 08:36 09:26 | 10 | 21:58:54 | -02:20:20 | m | | |
| 502214o | 1999 Sep 07 | 09:49 10:38 11:26 | 0.0 | 22:31:55 | -09:14:15 | m | 1999 RH ₂₁₅ | 03 |
| 502215o | 1999 Sep 07 | 09:54 10:43 11:31 | 0.0 | 22:35:33 | -08:52:51 | g | | |
| 502216o | 1999 Sep 07 | 09:59 10:48 11:35 | 0.0 | 22:39:11 | -08:31:00 | m | | |
| 502217o | 1999 Sep 07 | 10:04 10:53 11:40 | 0.0 | 22:42:48 | -08:09:16 | g | | |
| 502218o | 1999 Sep 07 | 10:09 10:58 11:45 | 0.0 | 22:46:25 | -07:47:36 | g | | |
| 502219o | 1999 Sep 07 | 10:14 11:02 11:50 | 10 | 22:31:55 | 00:45:35 | g | 1999 RJ ₂₁₅ | 00 |
| 502220o | 1999 Sep 07 | 10:18 11:07 11:55 | 10 | 22:35:33 | 01:07:24 | g | | |
| 502221o | 1999 Sep 07 | 10:23 11:12 11:59 | 10 | 22:39:11 | 01:28:59 | m | | |
| 502222o | 1999 Sep 07 | 10:28 11:17 12:04 | 10 | 22:42:29 | 01:50:25 | g | | |

Table 3—Continued

| ID | UT date | UT times | | | β ^a | α ^b | δ ^c | θ ^d | Objects | Chip |
|---------|-------------|----------|-------|-------|----------------------|-----------------------|-----------------------|-----------------------|------------------------|------|
| 502223o | 1999 Sep 07 | 10:33 | 11:21 | 12:09 | 10 | 22:46:26 | 02:12:36 | g | | |
| 502244o | 1999 Sep 07 | 12:15 | 13:11 | 14:10 | -10 | 00:45:17 | -05:08:23 | m | 1999 RK ₂₁₅ | 02 |
| | | | | | | | | | 1999 RN ₂₁₅ | 11 |
| 502245o | 1999 Sep 07 | 12:20 | 13:26 | 14:15 | -10 | 00:48:55 | -04:45:08 | m | | |
| 502246o | 1999 Sep 07 | 12:25 | 13:31 | 14:20 | -10 | 00:52:35 | -04:22:30 | p | | |
| 502247o | 1999 Sep 07 | 12:29 | 13:36 | 14:25 | -10 | 00:56:15 | -03:59:34 | m | | |
| 502248o | 1999 Sep 07 | 12:34 | 13:41 | 14:30 | 0.0 | 00:45:16 | 04:51:49 | m | 1999 RR ₂₁₅ | 09 |
| 502249o | 1999 Sep 07 | 12:39 | 13:46 | 14:34 | 0.0 | 00:48:55 | 05:14:52 | m | 1999 RT ₂₁₅ | 02 |
| 502250o | 1999 Sep 07 | 12:44 | 13:51 | 14:39 | 0.0 | 00:52:34 | 05:37:50 | m | 1999 RU ₂₁₅ | 04 |
| 502251o | 1999 Sep 07 | 12:48 | 13:55 | 14:44 | 10 | 00:45:16 | 14:51:49 | g | 1999 RV ₂₁₅ | 01 |
| | | | | | | | | | 1999 RW ₂₁₅ | 03 |
| 502252o | 1999 Sep 07 | 12:53 | 14:00 | 14:49 | 10 | 00:48:55 | 15:14:26 | m | | |
| 502253o | 1999 Sep 07 | 12:59 | 14:05 | 14:54 | 10 | 00:52:35 | 15:37:50 | m | | |
| 502367o | 1999 Sep 08 | 06:19 | 07:45 | 08:55 | -10 | 21:25:14 | -25:09:59 | p | | |
| 502368o | 1999 Sep 08 | 06:23 | 07:50 | 09:00 | -10 | 21:29:00 | -24:51:34 | p | | |
| 502371o | 1999 Sep 08 | 06:43 | 07:55 | 09:05 | -10 | 21:32:47 | -24:33:37 | p | | |
| 502372o | 1999 Sep 08 | 06:48 | 08:00 | 09:10 | -10 | 21:36:32 | -24:15:13 | p | | |
| 502374o | 1999 Sep 08 | 06:59 | 08:15 | 09:30 | -0.5 | 21:36:32 | -14:45:24 | m | | |
| 502375o | 1999 Sep 08 | 07:04 | 08:20 | 09:35 | -0.5 | 21:40:17 | -14:26:37 | p | 1999 RX ₂₁₅ | 07 |
| 502376o | 1999 Sep 08 | 07:09 | 08:25 | 09:40 | -0.5 | 21:47:45 | -13:48:24 | p | | |
| 502377o | 1999 Sep 08 | 07:14 | 08:30 | 09:46 | -0.5 | 21:51:29 | -13:29:14 | p | 1999 RY ₂₁₅ | 01 |
| | | | | | | | | | 1999 RZ ₂₅₃ | 03 |
| 502378o | 1999 Sep 08 | 07:19 | 08:34 | 09:54 | -10 | 21:40:17 | -23:56:27 | p | | |
| 502379o | 1999 Sep 08 | 07:23 | 08:39 | 09:59 | -10 | 21:44:01 | -23:37:32 | p | | |
| 502380o | 1999 Sep 08 | 07:28 | 08:43 | 10:03 | -10 | 21:47:45 | -23:18:24 | p | 1999 RZ ₂₁₅ | 06 |
| 502381o | 1999 Sep 08 | 07:33 | 08:51 | 10:08 | -10 | 21:51:28 | -22:59:04 | p | | |
| 502422o | 1999 Sep 08 | 11:21 | 12:23 | 13:30 | 9.5 | 23:33:18 | 06:36:36 | p | | |
| 502423o | 1999 Sep 08 | 11:26 | 12:28 | 13:35 | 9.5 | 23:36:53 | 06:59:39 | m | | |
| 502424o | 1999 Sep 08 | 11:31 | 12:32 | 13:40 | 9.5 | 23:40:27 | 07:23:07 | p | | |
| 502425o | 1999 Sep 08 | 11:36 | 12:37 | 13:44 | 0.5 | 23:33:13 | -02:23:38 | p | 1999 RA ₂₁₆ | 09 |
| 502426o | 1999 Sep 08 | 11:41 | 12:42 | 13:47 | 0.5 | 23:36:48 | -02:00:38 | m | | |
| 502427o | 1999 Sep 08 | 11:45 | 12:46 | 13:52 | 0.5 | 23:40:24 | -01:37:25 | p | 1999 RB ₂₁₆ | 07 |
| | | | | | | | | | 1999 RC ₂₁₆ | 11 |
| 502428o | 1999 Sep 08 | 11:53 | 12:51 | 13:57 | 9.5 | 23:44:04 | 07:46:06 | p | | |
| 502429o | 1999 Sep 08 | 11:58 | 13:08 | 14:50 | 9.5 | 23:47:39 | 08:09:21 | p | | |
| 502430o | 1999 Sep 08 | 12:04 | 13:13 | 14:55 | 9.5 | 23:51:13 | 08:32:54 | p | | |

Table 3—Continued

| ID | UT date | UT times | β ^a | α ^b | δ ^c | θ ^d | Objects | Chip |
|---------|-------------|-------------------|----------------------|-----------------------|-----------------------|-----------------------|------------------------|------|
| 502431o | 1999 Sep 08 | 12:09 13:17 15:00 | 9.5 | 23:54:49 | 08:56:14 | p | | |
| 502432o | 1999 Sep 08 | 12:13 13:22 15:05 | 9.5 | 23:58:25 | 09:19:24 | p | | |
| 502433o | 1999 Sep 08 | 12:18 13:26 15:10 | 9.5 | 00:01:59 | 09:42:57 | p | | |
| 527173o | 2000 Mar 31 | 09:42 10:42 11:32 | 20 | 11:51:06 | 20:57:55 | g | | |
| 527174o | 2000 Mar 31 | 09:53 10:46 11:37 | 0.0 | 11:51:06 | 00:57:54 | g | 2000 FX ₅₃ | 05 |
| 527175o | 2000 Mar 31 | 09:59 10:52 11:41 | 0.0 | 11:53:30 | 00:42:16 | m | | |
| 527176o | 2000 Mar 31 | 10:04 10:56 11:46 | 0.0 | 11:55:54 | 00:26:38 | p | | |
| 527301o | 2000 Apr 02 | 08:45 09:40 10:45 | 20 | 12:00:43 | 19:55:32 | m | | |
| 527302o | 2000 Apr 02 | 08:50 09:46 10:50 | 20 | 12:03:07 | 19:39:45 | m | | |
| 527303o | 2000 Apr 02 | 08:56 09:51 10:55 | 20 | 12:05:31 | 19:24:09 | m | | |
| 527304o | 2000 Apr 02 | 09:02 09:55 11:00 | 20 | 12:07:55 | 19:08:32 | m | | |
| 527305o | 2000 Apr 02 | 09:08 10:01 11:05 | 0.0 | 12:00:43 | -00:04:37 | g | | |
| 527306o | 2000 Apr 02 | 09:13 10:06 11:10 | 0.0 | 12:03:07 | -00:20:15 | m | 1994 GV ₉ | 11 |
| 527307o | 2000 Apr 02 | 09:19 10:19 11:15 | 0.0 | 12:05:30 | -00:35:51 | m | 2000 GK ₁₄₇ | 11 |
| 527308o | 2000 Apr 02 | 09:24 10:28 11:21 | 0.0 | 12:07:55 | -00:51:28 | p | | |
| 527309o | 2000 Apr 02 | 09:31 10:33 11:27 | 20 | 12:10:18 | 18:52:57 | p | | |
| 527310o | 2000 Apr 02 | 09:36 10:38 11:33 | 20 | 12:12:43 | 18:37:21 | p | | |
| 527455o | 2000 Apr 03 | 08:31 09:21 10:12 | 20 | 12:31:55 | 16:33:22 | m | 2000 GM ₁₄₇ | 03 |
| 527456o | 2000 Apr 03 | 08:36 09:26 10:17 | 20 | 12:34:19 | 16:17:59 | g | | |
| 527457o | 2000 Apr 03 | 08:41 09:31 10:23 | 20 | 12:36:43 | 16:02:37 | g | | |
| 527458o | 2000 Apr 03 | 08:46 09:36 10:34 | 0.0 | 12:31:55 | -03:26:38 | g | 2000 GW ₁₄₆ | 09 |
| 527459o | 2000 Apr 03 | 08:51 09:41 10:39 | 0.0 | 12:34:19 | -03:42:01 | m | 2000 GY ₁₄₆ | 04 |
| | | | | | | | 2000 GX ₁₄₆ | 06 |
| 527460o | 2000 Apr 03 | 08:56 09:46 10:44 | 0.0 | 12:36:43 | -03:57:23 | m | | |
| 527461o | 2000 Apr 03 | 09:01 09:51 10:49 | 0.0 | 12:39:07 | -04:12:43 | g | | |
| 527462o | 2000 Apr 03 | 09:06 09:57 10:55 | 20 | 12:39:07 | 15:47:17 | p | | |
| 527463o | 2000 Apr 03 | 09:11 10:02 11:00 | 20 | 12:41:31 | 15:31:59 | g | | |
| 527464o | 2000 Apr 03 | 09:16 10:07 11:05 | 20 | 12:43:56 | 15:16:43 | g | | |

Table 3—Continued

| ID | UT date | UT times | β ^a | α ^b | δ ^c | θ ^d | Objects | Chip |
|---------|-------------|-------------------|----------------------|-----------------------|-----------------------|-----------------------|------------------------|------|
| 527487o | 2000 Apr 03 | 11:22 12:16 13:16 | 0.0 | 13:54:20 | -11:43:09 | m | | |
| 527488o | 2000 Apr 03 | 11:26 12:22 13:21 | 0.0 | 13:56:48 | -11:56:34 | m | | |
| 527489o | 2000 Apr 03 | 11:32 12:27 13:26 | 20 | 13:54:20 | 08:16:52 | m | | |
| 527500o | 2000 Apr 03 | 12:32 13:32 14:10 | 20 | 13:56:48 | 08:03:26 | m | | |
| 527491o | 2000 Apr 03 | 11:45 12:37 13:37 | 20 | 13:59:16 | 07:50:04 | g | | |
| 527492o | 2000 Apr 03 | 11:50 12:42 13:42 | 20 | 14:01:44 | 07:36:48 | m | | |
| 527493o | 2000 Apr 03 | 11:55 12:48 13:47 | 20 | 14:04:13 | 07:23:38 | m | | |
| 527494o | 2000 Apr 03 | 12:00 12:53 13:52 | 20 | 14:06:41 | 07:10:32 | m | | |
| 527495o | 2000 Apr 03 | 12:05 12:59 13:58 | 0.0 | 14:04:13 | -12:36:23 | p | 2000 GZ ₁₄₆ | 11 |
| 527496o | 2000 Apr 03 | 12:11 13:04 14:03 | 0.0 | 14:06:41 | -12:49:28 | p | | |

Note. — This table lists fields imaged with the CFHT 12k Mosaic camera. Fields were imaged in triplets, with UT times given for each image. KBOs found are listed after the field of discovery. If more than one KBO was found in each field, they are listed on successive lines. The complete version of this table is in the electronic edition of the Journal. The printed edition contains only a sample.

^aJ2000 ecliptic latitude, degrees

^bJ2000 right ascension, hours

^cJ2000 declination, degrees

^dSeeing category: g, m, p represent the good (≤ 0.8 arc sec), medium (> 0.8 arc sec and < 1.0 arc sec), and poor (≥ 1.0 arc sec) seeing cases, respectively. The efficiency functions for each of these cases are presented in Table 4.

Table 4. CFHT Survey Efficiency

| Quantity | Good | Medium | Poor | Global |
|---------------------|-----------|-----------|-----------|-----------|
| Median PSF FWHM ["] | 0.76 | 0.90 | 1.07 | 0.84 |
| PSF FWHM Range ["] | 0.56–0.80 | 0.80–0.99 | 1.00–1.40 | 0.56–1.40 |
| e_{\max} | 0.83 | 0.83 | 0.83 | 0.83 |
| m_{R50} | 24.01 | 23.64 | 23.35 | 23.74 |
| σ | 0.29 | 0.38 | 0.47 | 0.48 |
| Fields Imaged | 95 | 89 | 49 | 233 |

Table 5. CFHT Discovery Conditions

| code | β [deg] | Date | R [AU] | Δ [AU] | α' [deg] | $m_R \pm \sigma$ | $m_R(1, 1, 0)$ | D [km] | MPC name |
|--------|------------------|------------|-------------|------------------|--------------------|------------------|----------------|-------------|------------------------|
| C17000 | +10 | 1999 02 15 | 41.161 | 42.085 | 0.5 | 21.36 ± 0.15 | 5.16 | 527 | 1999 CC ₁₅₈ |
| C71710 | 0.0 | 1999 02 10 | 47.562 | 48.474 | 0.4 | 21.08 ± 0.17 | 4.27 | 797 | 1999 CD ₁₅₈ |
| C72105 | 0.0 | 1999 02 10 | 37.694 | 38.631 | 0.5 | 22.80 ± 0.09 | 6.99 | 228 | 1999 CV ₁₁₈ |
| C72505 | 0.0 | 1999 02 10 | 46.521 | 47.477 | 0.3 | 23.54 ± 0.32 | 6.82 | 246 | 1999 CP ₁₅₃ |
| C72600 | 0.0 | 1999 02 10 | 37.713 | 38.671 | 0.4 | 23.76 ± 0.14 | 7.94 | 146 | 1999 CK ₁₅₈ |
| C75803 | 0.0 | 1999 02 10 | 34.141 | 35.053 | 0.6 | 23.61 ± 0.13 | 8.22 | 129 | 1999 CY ₁₁₈ |
| C75905 | 0.0 | 1999 02 10 | 45.106 | 46.010 | 0.5 | 24.40 ± 0.27 | 7.82 | 155 | 1999 CZ ₁₁₈ |
| C76103 | 0.0 | 1999 02 10 | 44.262 | 45.153 | 0.5 | 24.11 ± 0.26 | 7.61 | 171 | 1999 CA ₁₁₉ |
| C76104 | 0.0 | 1999 02 10 | 42.565 | 43.455 | 0.6 | 24.05 ± 0.21 | 7.72 | 162 | 1999 CW ₁₁₈ |
| C76107 | 0.0 | 1999 02 10 | 40.298 | 41.190 | 0.6 | 22.65 ± 0.07 | 6.55 | 278 | 1999 CB ₁₁₉ |
| C76207 | 0.0 | 1999 02 10 | 43.531 | 44.415 | 0.6 | 22.97 ± 0.06 | 6.54 | 280 | 1999 CC ₁₁₉ |
| C76502 | 0.0 | 1999 02 10 | 44.301 | 45.161 | 0.6 | 23.56 ± 0.14 | 7.06 | 220 | 1999 CD ₁₁₉ |
| C76609 | 0.0 | 1999 02 10 | 44.002 | 44.852 | 0.6 | 24.11 ± 0.11 | 7.64 | 169 | 1999 CX ₁₁₈ |
| C76800 | 0.0 | 1999 02 10 | 28.873 | 29.711 | 1.0 | 23.19 ± 0.04 | 8.52 | 112 | 1999 CE ₁₁₉ |
| C76907 | 0.0 | 1999 02 10 | 42.953 | 43.778 | 0.7 | 23.96 ± 0.08 | 7.59 | 172 | 1999 CW ₁₃₁ |
| C79710 | +0.5 | 1999 02 10 | — | — | — | 23.35 ± 0.14 | — | — | lost |
| C79900 | +0.5 | 1999 02 10 | — | — | — | 22.78 ± 0.12 | — | — | lost |
| C85003 | +0.5 | 1999 02 11 | — | — | — | 23.68 ± 0.13 | — | — | lost |
| C85110 | +0.5 | 1999 02 10 | 38.774 | 39.705 | 0.5 | 22.75 ± 0.20 | 6.82 | 246 | 1999 CF ₁₁₉ |
| C85200 | +0.5 | 1999 02 10 | 41.806 | 42.739 | 0.4 | 23.63 ± 0.07 | 7.37 | 191 | 1999 CG ₁₁₉ |
| C85204 | +0.5 | 1999 02 10 | 32.938 | 33.875 | 0.5 | 21.85 ± 0.09 | 6.61 | 271 | 1999 CL ₁₅₈ |
| C85300 | +0.5 | 1999 02 10 | 45.906 | 46.845 | 0.4 | 23.88 ± 0.23 | 7.22 | 204 | 1999 CH ₁₁₉ |
| C85404 | +0.5 | 1999 02 10 | 42.175 | 43.122 | 0.4 | 23.98 ± 0.08 | 7.68 | 165 | 1999 CS ₁₅₃ |
| C85410 | +0.5 | 1999 02 11 | — | — | — | 23.82 ± 0.08 | — | — | lost |
| C85504 | +0.5 | 1999 02 10 | 41.130 | 42.082 | 0.4 | 24.24 ± 0.16 | 8.05 | 139 | 1999 CK ₁₁₉ |
| C85509 | +0.5 | 1999 02 10 | 41.450 | 42.400 | 0.4 | 23.03 ± 0.12 | 6.80 | 247 | 1999 CJ ₁₁₉ |
| C85600 | +0.5 | 1999 02 10 | 45.773 | 46.727 | 0.3 | 22.52 ± 0.03 | 5.87 | 381 | 1999 CL ₁₁₉ |
| C85700 | +0.5 | 1999 02 10 | 41.159 | 42.117 | 0.3 | 23.25 ± 0.10 | 7.05 | 220 | 1999 CM ₁₁₉ |
| C85808 | +0.5 | 1999 02 10 | 45.122 | 46.085 | 0.3 | 23.41 ± 0.12 | 6.82 | 246 | 1999 CG ₁₅₄ |
| C85904 | +0.5 | 1999 02 10 | 43.697 | 44.664 | 0.3 | 23.96 ± 0.24 | 7.51 | 179 | 1999 CN ₁₁₉ |
| C85907 | +0.5 | 1999 02 10 | 42.168 | 43.135 | 0.3 | 22.96 ± 0.10 | 6.66 | 264 | 1999 CX ₁₃₁ |
| C85909 | +0.5 | 1999 02 11 | — | — | — | 23.99 ± 0.05 | — | — | lost |
| C88505 | 0.0 | 1999 02 10 | 40.502 | 41.482 | 0.2 | 23.11 ± 0.21 | 6.98 | 228 | 1999 CM ₁₅₃ |
| C88600 | 0.0 | 1999 02 10 | 37.016 | 37.995 | 0.2 | 23.61 ± 0.07 | 7.87 | 151 | 1999 CY ₁₃₁ |
| C88608 | 0.0 | 1999 02 11 | — | — | — | 23.64 ± 0.33 | — | — | lost |
| C88902 | 0.0 | 1999 02 10 | 41.998 | 42.968 | 0.2 | 23.99 ± 0.08 | 7.71 | 163 | 1999 CZ ₁₃₁ |

Table 5—Continued

| code | β [deg] | Date | R [AU] | Δ [AU] | α' [deg] | $m_R \pm \sigma$ | $m_R(1, 1, 0)$ | D [km] | MPC name |
|---------------------|------------------|------------|-------------|------------------|--------------------|------------------|----------------|-------------|------------------------|
| C88905 | 0.0 | 1999 02 11 | — | — | — | 24.20 ± 0.28 | — | — | lost |
| C89000 | 0.0 | 1999 02 10 | 42.306 | 43.273 | 0.3 | 23.75 ± 0.14 | 7.44 | 185 | 1999 CN ₁₅₃ |
| C89301 | 0.0 | 1999 02 10 | 38.704 | 39.660 | 0.4 | 22.91 ± 0.26 | 6.97 | 229 | 1999 CA ₁₃₂ |
| C89500 | 0.0 | 1999 02 10 | 43.383 | 44.330 | 0.4 | 23.99 ± 0.04 | 7.57 | 173 | 1999 CQ ₁₅₃ |
| C89503 ^a | 0.0 | 1999 02 10 | 44.241 | 45.187 | 0.4 | 23.24 ± 0.11 | 6.73 | 256 | 1995 DC ₀₂ |
| C89507 | 0.0 | 1999 02 10 | 30.805 | 31.752 | 0.5 | 22.11 ± 0.09 | 7.15 | 211 | 1999 CP ₁₃₃ |
| C92411 | -0.5 | 1999 02 10 | 27.797 | 28.719 | 0.7 | 21.89 ± 0.22 | 7.38 | 190 | 1999 CM ₁₅₈ |
| C98602 | -0.5 | 1999 02 12 | 43.113 | 44.031 | 0.5 | 22.96 ± 0.10 | 6.57 | 276 | 1999 CQ ₁₃₃ |
| C98603 | -0.5 | 1999 02 12 | 39.970 | 40.889 | 0.5 | 22.95 ± 0.17 | 6.88 | 239 | 1999 CO ₁₅₃ |
| C98703 | -0.5 | 1999 02 12 | 41.324 | 42.250 | 0.5 | 23.85 ± 0.14 | 7.64 | 168 | 1999 CR ₁₃₃ |
| C99411 | -0.5 | 1999 02 12 | 41.457 | 42.418 | 0.3 | 23.19 ± 0.18 | 6.97 | 229 | 1999 CU ₁₅₃ |
| C99502 | -0.5 | 1999 02 12 | 42.006 | 42.970 | 0.3 | 23.73 ± 0.25 | 7.45 | 184 | 1999 CH ₁₅₄ |
| C04700 | 0 | 1999 09 06 | 42.054 | 42.964 | 0.6 | 23.83 ± 0.25 | 7.54 | 176 | 1999 RS ₂₁₄ |
| C04707 | 0 | 1999 09 06 | 39.838 | 40.754 | 0.6 | 23.49 ± 0.14 | 7.45 | 184 | 1999 RT ₂₁₄ |
| C04910 | 0 | 1999 09 06 | 44.240 | 45.167 | 0.5 | 22.96 ± 0.23 | 6.45 | 291 | 1999 RU ₂₁₄ |
| C05105 | 0 | 1999 09 06 | 47.685 | 48.626 | 0.4 | 24.08 ± 0.20 | 7.26 | 201 | 1999 RV ₂₁₄ |
| C09804 | 0 | 1999 09 06 | 41.990 | 42.944 | 0.4 | 23.47 ± 0.34 | 7.19 | 207 | 1999 RW ₂₁₄ |
| C10300 | 0 | 1999 09 06 | 44.694 | 45.621 | 0.5 | 22.90 ± 0.20 | 6.36 | 304 | 1999 RX ₂₁₄ |
| C10801 | +10 | 1999 09 06 | 36.884 | 37.776 | 0.7 | 22.76 ± 0.08 | 7.03 | 223 | 1999 RY ₂₁₄ |
| C10908 | +10 | 1999 09 06 | 39.016 | 39.906 | 0.7 | 23.42 ± 0.10 | 7.46 | 183 | 1999 RZ ₂₁₄ |
| C13601 | 0 | 1999 09 06 | 30.686 | 31.610 | 0.7 | 23.71 ± 0.22 | 8.78 | 99 | 1999 RB ₂₁₅ |
| C13604 | 0 | 1999 09 06 | 42.465 | 43.380 | 0.5 | 22.88 ± 0.15 | 6.55 | 279 | 1999 RC ₂₁₅ |
| C14209 | +10 | 1999 09 06 | 37.824 | 38.692 | 0.8 | 23.08 ± 0.11 | 7.24 | 202 | 1999 RD ₂₁₅ |
| C18604 | 0 | 1999 09 07 | 41.618 | 42.588 | 0.4 | 22.57 ± 0.17 | 6.32 | 309 | 1999 RE ₂₁₅ |
| C18606 | 0 | 1999 09 07 | 43.000 | 43.964 | 0.4 | 22.95 ± 0.07 | 6.57 | 276 | 1999 RF ₂₁₅ |
| C21502 | 0 | 1999 09 07 | 44.015 | 45.017 | 0.2 | 23.49 ± 0.13 | 6.98 | 228 | 1999 RG ₂₁₅ |
| C21903 | +10 | 1999 09 07 | 36.161 | 37.154 | 0.3 | 23.91 ± 0.21 | 8.27 | 126 | 1999 RH ₂₁₅ |
| C22100 | +10 | 1999 09 07 | 34.047 | 35.041 | 0.3 | 22.42 ± 0.08 | 7.03 | 223 | 1999 RJ ₂₁₅ |
| C24402 | -10 | 1999 09 07 | 42.041 | 42.952 | 0.6 | 23.33 ± 0.11 | 7.04 | 222 | 1999 RK ₂₁₅ |
| C24411 | -10 | 1999 09 07 | 43.966 | 44.869 | 0.6 | 23.02 ± 0.11 | 6.56 | 277 | 1999 RN ₂₁₅ |
| C24809 | 0 | 1999 09 07 | 39.498 | 40.391 | 0.7 | 23.93 ± 0.07 | 7.91 | 148 | 1999 RR ₂₁₅ |
| C24902 | 0 | 1999 09 07 | 42.205 | 43.089 | 0.6 | 23.12 ± 0.19 | 6.83 | 245 | 1999 RT ₂₁₅ |
| C25004 | 0 | 1999 09 07 | 39.515 | 40.383 | 0.7 | 22.87 ± 0.20 | 6.82 | 245 | 1999 RU ₂₁₅ |
| C25101 | +10 | 1999 09 07 | 35.622 | 36.466 | 0.9 | 23.73 ± 0.19 | 8.16 | 132 | 1999 RV ₂₁₅ |
| C25103 | +10 | 1999 09 07 | 32.291 | 33.139 | 1.0 | 23.31 ± 0.16 | 8.17 | 132 | 1999 RW ₂₁₅ |
| C37507 | -0.5 | 1999 09 08 | 41.130 | 42.059 | 0.5 | 23.42 ± 0.16 | 7.23 | 203 | 1999 RX ₂₁₅ |

Table 5—Continued

| code | β [deg] | Date | R [AU] | Δ [AU] | α' [deg] | $m_R \pm \sigma$ | $m_R(1, 1, 0)$ | D [km] | MPC name |
|---------------------|------------------|------------|-------------|------------------|--------------------|------------------|----------------|-------------|------------------------|
| C37701 | -0.5 | 1999 09 08 | 36.314 | 37.262 | 0.5 | 22.25 ± 0.12 | 6.60 | 272 | 1999 RY ₂₁₅ |
| C37703 | -0.5 | 1999 09 08 | 39.955 | 40.905 | 0.5 | 22.04 ± 0.12 | 5.97 | 364 | 1999 RZ ₂₅₃ |
| C38006 | -10 | 1999 09 08 | 30.068 | 30.976 | 0.8 | 22.24 ± 0.16 | 7.40 | 188 | 1999 RZ ₂₁₅ |
| C41409 | +0.5 | 1999 09 08 | 42.379 | 43.377 | 0.2 | 23.08 ± 0.17 | 6.74 | 255 | 1999 RA ₂₁₆ |
| C41607 | +0.5 | 1999 09 08 | 33.725 | 34.718 | 0.3 | 22.42 ± 0.11 | 7.05 | 221 | 1999 RB ₂₁₆ |
| C41611 | +0.5 | 1999 09 08 | 46.992 | 47.985 | 0.2 | 23.56 ± 0.11 | 6.79 | 249 | 1999 RC ₂₁₆ |
| D17405 | 0.0 | 2000 03 31 | 37.749 | 38.722 | 0.3 | 23.33 ± 0.16 | 7.51 | 179 | 2000 FX ₅₃ |
| D30611 ^a | 0.0 | 2000 04 02 | 41.298 | 42.278 | 0.3 | 23.39 ± 0.10 | 7.18 | 208 | 1994 GV ₉ |
| D30711 | 0.0 | 2000 04 02 | 33.551 | 34.532 | 0.3 | 23.56 ± 0.12 | 8.24 | 127 | 2000 GK ₁₄₇ |
| D45503 | +20 | 2000 04 03 | 37.051 | 37.976 | 0.6 | 22.52 ± 0.20 | 6.78 | 250 | 2000 GM ₁₄₇ |
| D45809 | 0.0 | 2000 04 03 | 40.209 | 41.205 | 0.1 | 23.81 ± 0.15 | 7.71 | 163 | 2000 GW ₁₄₆ |
| D45904 | 0.0 | 2000 04 03 | 43.753 | 44.750 | 0.1 | 23.85 ± 0.11 | 7.40 | 188 | 2000 GY ₁₄₆ |
| D45906 | 0.0 | 2000 04 03 | 43.605 | 44.602 | 0.1 | 23.18 ± 0.11 | 6.74 | 255 | 2000 GX ₁₄₆ |
| D49511 | 0.0 | 2000 04 03 | 42.935 | 43.878 | 0.4 | 23.36 ± 0.15 | 6.99 | 228 | 2000 GZ ₁₄₆ |

^aThese are previously known objects serendipitously imaged in survey fields.

Note. — m_R is the red magnitude of the object, with 1 sigma error σ . $m_R(1, 1, 0)$ is the limiting red magnitude at geocentric distance $\Delta = 1$ AU, heliocentric distance $R = 1$ AU, and phase angle $\alpha' = 0$, computed from discovery geometry. Diameter D is computed directly from $m_R(1, 1, 0)$ via Equation 4, assuming $p \equiv 0.04$. Some quantities were not computed for lost objects because observations span only 2 hours.

Table 6. CFHT Orbital Elements

| code | a [AU] | e | i [deg] | Ω [deg] | ω [deg] | M [deg] | MJD | Δt | MPC name | sim ^b |
|---------------------|-------------|---------|--------------|-------------------|-------------------|--------------|-------|------------|------------------------|------------------|
| C17000 | 54.81897 | 0.29808 | 18.754 | 336.974 | 98.551 | 29.501 | 51800 | 2 | 1999 CC ₁₅₈ | |
| C71710 | 44.00641 | 0.15285 | 25.441 | 119.004 | 137.939 | 236.881 | 51800 | 2 | 1999 CD ₁₅₈ | i, q |
| C72105 | 52.82586 | 0.28892 | 5.467 | 305.621 | 148.820 | 16.449 | 51600 | 2 | 1999 CV ₁₁₈ | |
| C72505 | 45.15557 | 0.16213 | 3.038 | 122.823 | 247.176 | 100.913 | 51600 | 2 | 1999 CP ₁₅₃ | i, q |
| C72600 | 40.91130 | 0.06725 | 17.068 | 127.720 | 322.119 | 35.433 | 51800 | 2 | 1999 CK ₁₅₈ | i, q |
| C75803 | 89.81583 | 0.61493 | 25.619 | 163.125 | 15.456 | 357.553 | 51600 | 2 | 1999 CY ₁₁₈ | |
| C75905 | 110.36855 | 0.65629 | 27.804 | 345.177 | 235.542 | 350.265 | 51600 | 2 | 1999 CZ ₁₁₈ | |
| C76103 | 45.15314 | 0.0 | 0.283 | 24.858 | 319.882 | 181.758 | 51260 | (86) | 1999 CA ₁₁₉ | i, q |
| C76104 | 43.45475 | 0.0 | 0.819 | 154.471 | 173.481 | 198.705 | 51260 | (86) | 1999 CW ₁₁₈ | i, q |
| C76107 | 43.64467 | 0.05625 | 9.160 | 168.036 | 358.276 | 0.071 | 51240 | (62) | 1999 CB ₁₁₉ | i, q |
| C76207 | 44.44015 | 0.00127 | 0.458 | 190.261 | 272.993 | 65.792 | 51800 | 2 | 1999 CC ₁₁₉ | i, q |
| C76502 | 43.99328 | 0.02655 | 2.396 | 166.381 | 183.867 | 180.075 | 51240 | (62) | 1999 CD ₁₁₉ | i, q |
| C76609 | 43.66175 | 0.02725 | 1.784 | 175.714 | 175.748 | 180.064 | 51240 | (62) | 1999 CX ₁₁₈ | i, q |
| C76800 | 39.33216 | 0.24461 | 1.429 | 171.557 | 1.040 | 0.083 | 51240 | (58) | 1999 CE ₁₁₉ | |
| C76907 | 43.19444 | 0.01577 | 7.952 | 174.627 | 209.869 | 150.003 | 51600 | 2 | 1999 CW ₁₃₁ | i, q |
| C85110 | 91.70394 | 0.58203 | 19.700 | 303.437 | 203.636 | 354.915 | 51600 | 2 | 1999 CF ₁₁₉ | |
| C85200 | 51.35701 | 0.33914 | 16.656 | 304.264 | 257.457 | 317.562 | 51600 | 2 | 1999 CG ₁₁₉ | |
| C85204 | 41.77052 | 0.21889 | 10.025 | 120.074 | 325.711 | 26.075 | 51800 | 2 | 1999 CL ₁₅₈ | |
| C85300 | 43.39088 | 0.08942 | 19.968 | 122.349 | 156.415 | 210.747 | 51600 | 2 | 1999 CH ₁₁₉ | i, q |
| C85404 | 44.51143 | 0.11926 | 0.983 | 343.336 | 223.233 | 293.035 | 51600 | 2 | 1999 CS ₁₅₃ | i, q |
| C85504 | 42.08155 | 0.0 | 11.592 | 123.077 | 2.999 | 0.000 | 51220 | (8) | 1999 CK ₁₁₉ | i, q |
| C85509 | 45.42766 | 0.06934 | 3.200 | 313.350 | 189.726 | 346.285 | 51600 | 2 | 1999 CJ ₁₁₉ | i, q |
| C85600 | 46.95343 | 0.02034 | 23.292 | 125.157 | 284.096 | 76.274 | 51600 | 2 | 1999 CL ₁₁₉ | |
| C85700 | 44.41239 | 0.13382 | 2.744 | 118.490 | 294.453 | 61.472 | 51600 | 2 | 1999 CM ₁₁₉ | i, q |
| C85808 | 43.04996 | 0.08599 | 0.766 | 100.205 | 176.323 | 219.095 | 51600 | 2 | 1999 CG ₁₅₄ | i, q |
| C85904 | 43.89874 | 0.01744 | 0.997 | 347.227 | 323.092 | 180.915 | 51600 | 2 | 1999 CN ₁₁₉ | i, q |
| C85907 | 41.48466 | 0.18854 | 9.760 | 127.984 | 114.269 | 269.788 | 51600 | 2 | 1999 CX ₁₃₁ | |
| C88505 | 44.12661 | 0.05994 | 0.190 | 87.878 | 60.139 | 0.067 | 51240 | (57) | 1999 CM ₁₅₃ | i, q |
| C88600 | 43.92279 | 0.13496 | 25.167 | 148.245 | 0.110 | 359.999 | 51220 | (8) | 1999 CY ₁₃₁ | i, q |
| C88902 | 44.41005 | 0.03248 | 2.371 | 151.799 | 359.878 | 359.999 | 51220 | (8) | 1999 CZ ₁₃₁ | i, q |
| C89000 | 42.59212 | 0.01599 | 7.480 | 153.050 | 179.417 | 180.056 | 51240 | (56) | 1999 CN ₁₅₃ | i, q |
| C89301 | 43.96574 | 0.09794 | 12.071 | 154.871 | 0.530 | 0.067 | 51240 | (56) | 1999 CA ₁₃₂ | i, q |
| C89500 | 44.33005 | 0.0 | 0.208 | 181.177 | 336.136 | 0.000 | 51220 | (30) | 1999 CQ ₁₅₃ | i, q |
| C89503 ^a | 43.86806 | 0.06335 | 2.349 | 154.182 | 124.958 | 244.781 | 51200 | 5 | 1995 DC ₀₂ | i, q |
| C89507 | 39.21917 | 0.19335 | 2.946 | 333.980 | 171.178 | 8.172 | 51240 | (63) | 1999 CP ₁₃₃ | |
| C92411 | 39.37318 | 0.27060 | 9.242 | 338.951 | 182.862 | 0.078 | 51240 | (60) | 1999 CM ₁₅₈ | |

Table 6—Continued

| code | a [AU] | e | i [deg] | Ω [deg] | ω [deg] | M [deg] | MJD | Δt | MPC name | sim ^b |
|--------|-------------|---------|--------------|-------------------|-------------------|--------------|-------|------------|------------------------|------------------|
| C98602 | 41.38725 | 0.09152 | 13.265 | 123.288 | 220.788 | 131.912 | 51600 | 2 | 1999 CQ ₁₃₃ | i, q |
| C98603 | 43.76827 | 0.08381 | 0.805 | 278.110 | 162.704 | 36.595 | 51600 | 2 | 1999 CO ₁₅₃ | i, q |
| C98703 | 42.24989 | 0.0 | 1.727 | 135.130 | 347.987 | 0.000 | 51220 | (6) | 1999 CR ₁₃₃ | i, q |
| C99411 | 44.09712 | 0.04544 | 2.698 | 139.275 | 25.598 | 329.621 | 51600 | 2 | 1999 CU ₁₅₃ | i, q |
| C99502 | 43.36260 | 0.08425 | 0.843 | 164.676 | 54.980 | 282.282 | 51600 | 2 | 1999 CH ₁₅₄ | i, q |
| C04700 | 42.96436 | 0.0 | 3.174 | 139.496 | 178.818 | 0.000 | 51440 | (33) | 1999 RS ₂₁₄ | i, q |
| C04707 | 42.52058 | 0.04681 | 2.578 | 138.065 | 151.541 | 27.528 | 51800 | 2 | 1999 RT ₂₁₄ | i, q |
| C04910 | 95.52823 | 0.68200 | 4.169 | 137.804 | 261.582 | 345.449 | 51460 | (68) | 1999 RU ₂₁₄ | |
| C05105 | 45.03200 | 0.07981 | 1.149 | 144.629 | 357.831 | 180.129 | 51440 | (34) | 1999 RV ₂₁₄ | i, q |
| C09804 | 43.21204 | 0.07676 | 1.370 | 0.376 | 90.714 | 280.315 | 51800 | 2 | 1999 RW ₂₁₄ | i, q |
| C10300 | 44.90203 | 0.04172 | 4.818 | 3.793 | 247.094 | 111.571 | 51800 | 2 | 1999 RX ₂₁₄ | i, q |
| C10801 | 45.55261 | 0.18833 | 13.689 | 327.338 | 72.154 | 340.779 | 51800 | 2 | 1999 RY ₂₁₄ | |
| C10908 | 87.18745 | 0.57385 | 20.301 | 214.776 | 117.659 | 8.376 | 51460 | (65) | 1999 RZ ₂₁₄ | |
| C13601 | 48.31520 | 0.34575 | 7.814 | 4.997 | 1.548 | 0.096 | 51460 | (66) | 1999 RB ₂₁₅ | |
| C13604 | 44.33566 | 0.05693 | 1.399 | 189.037 | 249.705 | 295.722 | 51800 | 2 | 1999 RC ₂₁₅ | i, q |
| C14209 | 120.78728 | 0.68630 | 25.884 | 210.337 | 141.064 | 2.795 | 51800 | 2 | 1999 RD ₂₁₅ | |
| C18604 | 45.16729 | 0.11648 | 1.344 | 149.278 | 112.725 | 55.573 | 51800 | 2 | 1999 RE ₂₁₅ | i, q |
| C18606 | 43.96413 | 0.0 | 3.675 | 327.579 | 0.196 | 0.000 | 51460 | (65) | 1999 RF ₂₁₅ | i, q |
| C21502 | 47.46151 | 0.15843 | 0.252 | 294.642 | 122.868 | 298.384 | 51800 | 2 | 1999 RG ₂₁₅ | |
| C21903 | 43.79253 | 0.15198 | 10.212 | 276.873 | 68.428 | 357.760 | 51800 | 2 | 1999 RH ₂₁₅ | i |
| C22100 | 59.78767 | 0.42018 | 19.719 | 314.937 | 43.698 | 355.025 | 51800 | 2 | 1999 RJ ₂₁₅ | |
| C24402 | 39.72913 | 0.16644 | 11.499 | 137.761 | 103.443 | 110.966 | 51460 | (65) | 1999 RK ₂₁₅ | |
| C24411 | 43.21648 | 0.04096 | 12.404 | 140.634 | 68.292 | 159.483 | 51800 | 2 | 1999 RN ₂₁₅ | i |
| C24809 | 44.91243 | 0.10067 | 1.144 | 185.694 | 185.986 | 0.104 | 51460 | (65) | 1999 RR ₂₁₅ | i, q |
| C24902 | 43.08942 | 0.0 | 21.907 | 192.898 | 179.849 | 0.000 | 51460 | (63) | 1999 RT ₂₁₅ | i, q |
| C25004 | 43.59152 | 0.09467 | 7.718 | 14.298 | 316.918 | 36.841 | 51800 | 2 | 1999 RU ₂₁₅ | i, q |
| C25101 | 44.98636 | 0.18949 | 21.975 | 351.818 | 27.099 | 359.849 | 51800 | 2 | 1999 RV ₂₁₅ | |
| C25103 | 39.63957 | 0.24625 | 10.424 | 253.992 | 180.867 | 322.404 | 51460 | (63) | 1999 RW ₂₁₅ | |
| C37507 | 42.05898 | 0.0 | 0.894 | 99.349 | 223.581 | 0.000 | 51440 | (32) | 1999 RX ₂₁₅ | i, q |
| C37701 | 45.48866 | 0.24329 | 22.180 | 326.622 | 51.565 | 328.531 | 51800 | 2 | 1999 RY ₂₁₅ | |
| C37703 | 44.04333 | 0.11336 | 0.563 | 84.582 | 297.742 | 315.250 | 51800 | 2 | 1999 RZ ₂₅₃ | i, q |
| C38006 | 102.15245 | 0.69681 | 25.492 | 341.669 | 336.567 | 0.548 | 51800 | 2 | 1999 RZ ₂₁₅ | |
| C41409 | 44.62426 | 0.10334 | 0.787 | 192.150 | 80.444 | 69.830 | 51800 | 2 | 1999 RA ₂₁₆ | i, q |
| C41607 | 47.95883 | 0.29806 | 12.669 | 175.730 | 208.315 | 345.437 | 51800 | 2 | 1999 RB ₂₁₆ | |
| C41611 | 44.40277 | 0.08068 | 0.588 | 190.538 | 344.286 | 180.149 | 51460 | (62) | 1999 RC ₂₁₆ | i, q |
| D17405 | 43.19458 | 0.18511 | 4.799 | 175.196 | 68.292 | 312.820 | 51640 | (37) | 2000 FX ₅₃ | |

Table 6—Continued

| code | a [AU] | e | i [deg] | Ω [deg] | ω [deg] | M [deg] | MJD | Δt | MPC name | sim ^b |
|---------------------|-------------|---------|--------------|-------------------|-------------------|--------------|-------|------------|------------------------|------------------|
| D30611 ^a | 43.62227 | 0.06202 | 0.565 | 176.852 | 301.264 | 57.670 | 51800 | 7 | 1994 GV ₉ | i, q |
| D30711 | 39.40243 | 0.20660 | 7.164 | 1.681 | 243.983 | 316.246 | 51640 | (35) | 2000 GK ₁₄₇ | |
| D45503 | 39.58196 | 0.19165 | 18.077 | 96.123 | 173.826 | 292.969 | 51640 | (33) | 2000 GM ₁₄₇ | |
| D45809 | 41.20546 | 0.00000 | 28.975 | 8.913 | 179.957 | 0.000 | 51620 | (1) | 2000 GW ₁₄₆ | i, q |
| D45904 | 44.74976 | 0.0 | 2.718 | 13.462 | 134.077 | 42.017 | 51640 | (34) | 2000 GY ₁₄₆ | i, q |
| D45906 | 44.60190 | 0.0 | 0.664 | 344.290 | 204.949 | 0.066 | 51640 | (34) | 2000 GX ₁₄₆ | i, q |
| D49511 | 43.87783 | 0.00000 | 1.999 | 215.697 | 357.395 | 0.000 | 51620 | (2) | 2000 GZ ₁₄₆ | i, q |

Note. — This table lists the orbits of all objects discovered, excluding the 7 lost objects which had insufficient timebases (2 hours) to provide meaningful orbits. The Keplerian orbital elements a , e , i , Ω , ω , and M represent semimajor axis, eccentricity, inclination, longitude of ascending node, argument of perihelion, and mean anomaly, respectively. MJD is the Modified Julian Date of the orbit computation, and Δt is the timebase in oppositions (days). Orbital elements were computed independently by the Minor Planet Center and by David Tholen (Univ. of Hawaii).

^aThis known object was serendipitously imaged in survey fields.

^bThis column identifies simulation in which the object was used: q and/or i . All CKBOs were used in the i simulation, and all CKBOs discovered in ecliptic fields were used in the q simulation.

Table 7. CLF and DLF Computation

| m_R range ^a | N'_{DLF} ^b | N'_{CLF} ^c | $\bar{\varepsilon}$ ^d | N_{DLF} ^e | N_{CLF} ^f | Σ_{DLF} ^g | Σ_{CLF} ^h |
|--------------------------|--------------------------------|--------------------------------|----------------------------------|-------------------------------|-------------------------------|------------------------------------|------------------------------------|
| 21.0 – 21.5 | 1 | 1 | 0.83 | 1.2 | 1.2 | $0.03^{+0.05}_{-0.02}$ | $0.03^{+0.05}_{-0.02}$ |
| 21.5 – 22.0 | 2 | 3 | 0.83 | 2.4 | 3.6 | $0.06^{+0.06}_{-0.04}$ | $0.10^{+0.08}_{-0.04}$ |
| 22.0 – 22.5 | 4 | 7 | 0.83 | 4.8 | 8.5 | $0.13^{+0.08}_{-0.06}$ | $0.23^{+0.11}_{-0.07}$ |
| 22.5 – 23.0 | 16 | 23 | 0.80 | 19.9 | 28.4 | $0.54^{+0.13}_{-0.13}$ | $0.76^{+0.17}_{-0.15}$ |
| 23.0 – 23.5 | 18 | 41 | 0.70 | 25.9 | 54.2 | $0.70^{+0.16}_{-0.16}$ | $1.46^{+0.24}_{-0.22}$ |
| 23.5 – 24.0 | 25 | 66 | 0.34 | 73.8 | 128.1 | $1.98^{+0.40}_{-0.40}$ | $3.44^{+0.46}_{-0.46}$ |
| 24.0 – 24.5 | 7 | 73 | 0.11 | 63.3 | 191.4 | $1.70^{+0.74}_{-0.57}$ | $5.14^{+0.87}_{-0.73}$ |
| 24.5 – 25.0 | 1 | 74 | 0.02 | 46.2 | 237.5 | $1.24^{+1.86}_{-0.91}$ | $6.38^{+2.06}_{-1.17}$ |

^athe apparent red magnitude range

^bthe number of KBOs found within 0.5° of the ecliptic in the m_R range

^cthe cumulative number of ecliptic KBOs found

^dmean efficiency correction ε for the given m_R range

^ethe bias-corrected number of KBOs, computed by summing $1/\varepsilon$ (Equation 2) for all objects in the magnitude range

^fthe cumulative bias-corrected number of KBOs

^gthe bias-corrected surface density for the given magnitude range, equal to N_{DLF}/A , where $A = 37.2$ sq deg; errors are computed from 1σ Poisson errors for N'_{DLF}

^hthe bias-corrected cumulative surface density, errors are summed in quadrature from the Σ_{DLF} errors

Table 8. Classical KBO Size Distribution Model Parameters

| Symbol | Value | Distribution | Description |
|--|--------------|--------------------------------|---------------------------------------|
| a | 40.5 – 46 AU | $n(a)da \sim a^{1-p}da$ | semimajor axis |
| p^a | 2 | — | semimajor axis power |
| e | 0 – 0.25 | uniform | eccentricity |
| q' | $q' > 37$ AU | — | perihelion distance |
| i | 0 – 90 deg | Gaussian, $i_{1/2}$ half-width | inclination distribution |
| $i_{1/2}$ | 20 deg | — | Half-Width of the i distribution |
| ω | 0 – 360 deg | uniform | argument of perihelion |
| Ω | 0 – 360 deg | uniform | longitude of the ascending node |
| M | 0 – 360 deg | uniform | mean anomaly |
| r | 50 – 1000 km | $n(r)dr \sim r^{-q}dr$ | radius |
| q | fitted | — | size distribution index |
| p_R | 0.04 | — | geometric red albedo |
| $N_{\text{CKBOs}}(D > 100 \text{ km})$ | fitted | — | number of CKBOs with $D > 100$ km |
| — | 20 | — | number of radius bins (log intervals) |
| — | 50 — 1000 km | — | radius bin range |

^aIn the circular orbit case, p corresponds to the power of the decrease in ecliptic plane surface density Σ_{ecl} as a function of heliocentric distance R , $\Sigma_{\text{ecl}} \sim R^{-p}$.

Table 9. Selected Size Distribution Measurements of the KBOs

| m_R Range of Discovery | Number of KBOs found | q | Reference |
|-----------------------------|-------------------------|---------------------|--|
| 21.1 – 24.6 | 86 | $4.0^{+0.6}_{-0.5}$ | This Work |
| 25.5 – 27.2 ^a | 2 | 3.6 ± 0.1 | Chiang & Brown 1999 ^b |
| 23.8 – 26.7 | 6 | 3.7 ± 0.2 | Luu & Jewitt 1998 ^b |
| 23.0 – 25.8 | 5 | $4.8^{+0.5}_{-0.6}$ | Gladman et al. 1998 ^b |
| 20.6 – 23.0 | 13 | 4.0 ± 0.5 | Jewitt, Luu & Trujillo 1998 ^b |

^aV magnitude

^bExtrapolated from CLF slope, α , via Equation 3.

Table 10. Simple Inclination Model

| Ecliptic Latitude [deg] | 0 | 10 ^a | 20 |
|---|--|--|--|
| Number of Fields | 119 | 94 | 19 |
| Field Area [sq deg] | 37.2 | 29.8 | 6.0 |
| Number of KBOs | 74 | 11 | 1 |
| Surface Density [# / sq deg] ^b | 1.80 ^{+0.22} _{-0.20} | 0.34 ^{+0.12} _{-0.10} | 0.17 ^{+0.25} _{-0.12} |
| $R(10^\circ, 0^\circ)$ and $R(20^\circ, 0^\circ)$ | — | 0.19 ^{+0.07} _{-0.06} | 0.09 ^{+0.13} _{-0.07} |
| $i_{1/2}$ [deg] | | 14 ⁺⁶ ₋₃ | 19 ⁺²⁰ ₋₇ |

^aResults for ecliptic latitude $\beta = +10^\circ$ are consistent with those of $\beta = -10^\circ$, so were combined.

^bError bars were computed assuming Poisson detection statistics (Kraft, Burrows & Nousek 1991).

Table 11. KBO Inclination Model Parameters

| Symbol | Value | Distribution | Description |
|---------------------------------------|--------------|--------------------------------|------------------------------------|
| a | 40.5 – 46 AU | $n(a)da \sim a^{1-p}da$ | semimajor axis |
| p^a | 2 | — | semimajor axis power |
| e | 0 – 0.25 | uniform | eccentricity |
| q' | $q' > 37$ AU | — | perihelion distance |
| i | 0 – 90 deg | Gaussian, $i_{1/2}$ half-width | inclination distribution |
| $i_{1/2}$ | fitted | — | Half-Width of the i distribution |
| ω | 0 – 360 deg | uniform | argument of perihelion |
| Ω | 0 – 360 deg | uniform | longitude of the ascending node |
| M | 0 – 360 deg | uniform | mean anomaly |
| r | 50 – 1000 km | $n(r)dr \sim r^{-q}dr$ | radius |
| q | 3.7 | — | slope parameter |
| p_R | 0.04 | — | red albedo |
| $N_{\text{KBOs}}(D > 100 \text{ km})$ | fitted | — | number of CKBOs with $D > 100$ km |
| — | 45 | — | number of inclination bins |
| — | 0°— 90° | — | inclination bin range |

^aIn the circular orbit case, p corresponds to the power of the decrease in ecliptic plane surface density Σ_{ecl} as a function of heliocentric distance R , $\Sigma_{\text{ecl}} \sim R^{-p}$.

Table 12. Minimum q_{out} Needed
to Explain Observed Edge

| $r_{\text{min}}^{\text{a}}$ | q_{out} |
|-----------------------------|------------------|
| 50.0 | 10 |
| 25.0 | 7.4 |
| 12.5 | 6.2 |
| 6.3 | 5.6 |

^aMinimum radius [km] for which mass is conserved across the edge boundary.